Autogenous shrinkage of alkali-activated slag
A critical review

Li, Zhenming; Chen, Yun; Provis, John L.; Cizer, Özlem; Ye, Guang

DOI
10.1016/j.cemconres.2023.107244

Publication date
2023

Document Version
Final published version

Published in
Cement and Concrete Research

Cement and Concrete Research 172 (2023) 107244

Contents lists available at ScienceDirect

Cement and Concrete Research

journal homepage: www.elsevier.com/locate/cemconres

Autogenous shrinkage of alkali-activated slag: A critical review

Zhenming Li [a,b,*], Yun Chen [a,c], John L. Provis [b], Özlem Cizer [d], Guang Ye [a]

[a] Department of Materials, Mechanics, Management & Design, Faculty of Civil Engineering and Geoscience, Delft University of Technology, Delft, the Netherlands
[b] Department of Materials Science and Engineering, The University of Sheffield, Sheffield, United Kingdom
[c] School of Materials Science and Engineering, South China University of Technology, Guangzhou, Guangdong, China
[d] Department of Civil Engineering, Materials and Constructions, KU Leuven, Leuven, Belgium

ARTICLE INFO

Keywords:
Autogenous shrinkage
Alkali-activated slag
Mechanism
Modelling
Cracking
Mitigation

ABSTRACT

This paper provides a critical review on autogenous shrinkage of alkali-activated slag (AAS). It is reported that AAS paste, mortar, and concrete generally show larger autogenous shrinkage than Portland cement (PC) counterparts. Self-desiccation is the main driving force of the autogenous shrinkage of hardened AAS, but other mechanisms also play roles, particularly at early age. Existing models developed for PC do not give satisfactory estimations of the autogenous shrinkage of AAS, unless the pronounced viscoelasticity of AAS is considered. The susceptibility of AAS concrete to extensive cracking is not necessarily high due to the effects of stress relaxation, but local creep can exacerbate the development of microcracks. Various strategies have been proposed to mitigate the autogenous shrinkage of AAS, but many exhibit side effects, e.g., strength reduction. Existing testing methods for autogenous shrinkage of PC seem applicable to AAS, but the starting time and test duration need to be reconsidered.

1. Introduction

Alkali-activated materials (AAMs) have attracted increasing academic and industrial interest in recent decades [1–3]. An important motivation for the use of AAMs originates from their identified potential as greener alternatives to Portland cement (PC) [4]. Commercial-scale production of AAMs as binder materials is seen in different regions all over the world [5]. Currently, the most used precursors worldwide to synthesize AAMs are metallurgical slags (mainly ground granulated blast furnace slag), calcined clays, and fly ash from thermal power plants. Among these, slag-based AAMs are the dominant class of AAMs currently in large-scale production for concrete applications; fly ash availability is becoming limited in some regions, and calcined clay-based AAMs require further development in materials processing and durability assessment in the context of reinforced concretes.

Despite the potential advantages of alkali-activated slag (AAS) to make lower-carbon and durable concretes [6], the structural application of AAS-based systems is still limited, and part of the reason lies in the uncertainty that exists around the volumetric stability of these materials. An increasing number of publications are showing that AAS-based systems demonstrate greater shrinkage than their PC counterparts [7]; when restrained, this shrinkage can cause internal tensile stresses and bring a risk of macro/micro cracking. Restraint of the deformation of binder materials is almost ubiquitous in structural concretes, from both internal, e.g. aggregates and steel rebar, and external sources, e.g. ground or adjacent structures [8,9]. The occurrence of cracking in concrete can impair its mechanical properties and durability (Fig. 1). Furthermore, even in the absence of thorough cracking, the persistent presence of internal tensile stress induced by shrinkage can compound with other effects and result in a reduction in the load-bearing capacity of concrete. The current research status shows that the volumetric stability of AAS systems is one of the least satisfactory aspects among all performances, including the variability induced by different chemical compositions of precursor and activator (and admixtures), the reaction products and microstructure, mechanical properties and durability issues such as carbonation, freeze and thaw resistance, etc. [10–15]. The volume stability issue seems to deserve more research attention than it has received.

Autogenous shrinkage is defined as the self-created bulk shrinkage of a binder system [16]. Among the various types of deformations of binder materials, autogenous shrinkage plays an important role, not only because it develops rapidly at early age when the tensile strain capacity

* Corresponding author at: Department of Materials, Mechanics, Management & Design, Faculty of Civil Engineering and Geoscience, Delft University of Technology, Delft, the Netherlands.
E-mail address: Zhenming.li@sheffield.ac.uk (Z. Li).

https://doi.org/10.1016/j.cemconres.2023.107244
Received 13 January 2023; Received in revised form 16 June 2023; Accepted 20 June 2023
Available online 30 June 2023

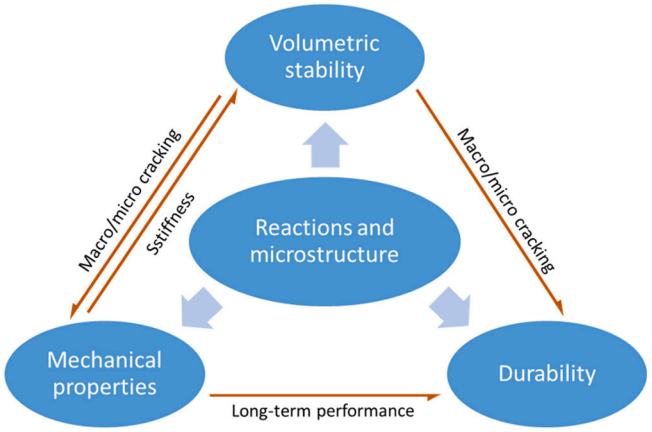

Fig. 1. Schematic representation of the hardened properties of binder materials.

of the material remains low, but also that it occurs without the need for substance (e.g., moisture) or heat exchange with the environment. Under drying conditions or thermal shock when drying shrinkage or thermal deformation takes place, autogenous shrinkage is still present and the consequent tensile stress can compound with those induced by drying and temperature change. According to the results from [17], the autogenous shrinkage accounts for 30 %–70 % of the total drying shrinkage of AAS mortar depending on the activator composition; while under sealed and non-isothermal condition, the autogenous shrinkage can be >2 times larger than the thermal shrinkage of AAS concrete [16], both indicating the significance of autogenous shrinkage. However, the number of publications to date concerning autogenous shrinkage (~80 papers according to the Scopus database) accounts for only a small part of those on all volume stability issues of AAS (~600 papers). Moreover, no review paper can be found focusing specifically on the autogenous shrinkage of AAS, although in some reviews the autogenous shrinkage was briefly discussed [7,10,18]. So, key questions around whether autogenous shrinkage is a problem for AAS as a binder material, and if so, how to solve this problem, remain unanswered for researchers and industrial users.

Against this background, this review critically assesses the existing knowledge and identifies future research directions on autogenous shrinkage of AAS. The slag concerned in this paper is ground granulated blast furnace slag unless noted. The outline of this paper is shown in Fig. 2, which identifies six key aspects requiring discussion. First, the magnitude of autogenous shrinkage of AAS systems and the influential factors are reported. The mechanisms of autogenous shrinkage proposed by researchers are then discussed. The respective applicability of various prediction models for autogenous shrinkage of AAS is reviewed. The cracking tendency of AAS paste, mortar and concrete due to restrained autogenous shrinkage is then evaluated, and some mitigation approaches are outlined. Some remarks are provided on the testing methods for autogenous shrinkage, which links back to the determination of the magnitude of autogenous shrinkage. The research gaps and outlook on future research are given in each section.

2. Magnitude and influential factors

The magnitude of autogenous shrinkage of AAS is influenced by various factors, including the properties of the slag used, the composition of the activator, and the presence or absence of other admixtures. While the chemical composition and reactivity of ground granulated blast furnace slag used in different studies vary in a small range, the type, alkalinity and water content of activators can differ dramatically.

Table A1 summarizes the literature reporting the magnitude of autogenous shrinkage of alkali-activated systems that use ground granulated blast furnace slag as the sole aluminosilicate precursor. The table is categorized based on the presence of aggregates and in each category the table is further sorted by the type and composition of activator and curing temperature. Since few studies were found on shrinkage of potassium-activated slag systems, the literature covered in this study is focused on the use of sodium as the activator cation. It can be seen that more shrinkage tests were conducted at paste and mortar scales than at concrete scale. Sodium silicate was the most widely used type of activator in autogenous shrinkage testing. Both linear and volumetric deformations were tested in the literature, while the length change of specimens in corrugated tubes was measured the most.

Based on these experimental results, the influences of Na_2O content and modulus of the sodium silicate activator on the autogenous shrinkage of AAS paste at 7 days are plotted in Fig. 3, with a constant water/binder (w/b) ratio of 0.4, which is the most often used w/b value in literature (see Table A1). A positive correlation between Na_2O content and autogenous shrinkage is identified in Fig. 3 when the modulus ranges from 0.5 to 1.5. This is plausible since a higher Na_2O content normally means a higher available alkalinity in the pore solution, which is desirable for the dissolution of slag and formation of reaction products [19]. The reaction rate can be therefore faster and the pore structure can be denser. These contribute to not only a higher compressive strength [20], but also a larger autogenous shrinkage, as will be elaborated in the

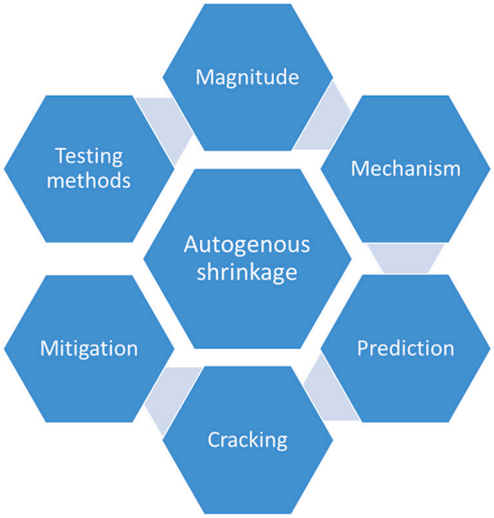

Fig. 2. Outline of this review.

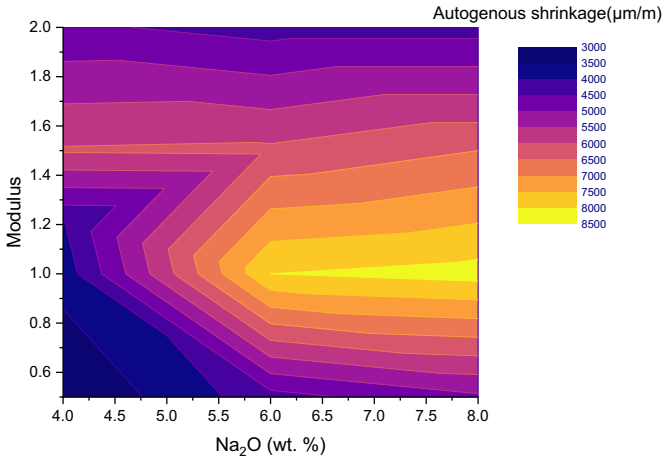

Fig. 3. Influences of modulus and Na_2O content of the sodium silicate activator on the autogenous shrinkage of AAS pastes at 7 days with a constant w/b ratio of 0.4. Data compiled from references [21–23].

next section.

By contrast, the influence of the activator modulus on the autogenous shrinkage of AAS paste is not monotonic. A modulus of around 1.0 leads to the highest autogenous shrinkage when the Na_2O content is above 5 %. A very high or very low modulus is favourable for a lower autogenous shrinkage, but it also leads to lower strength [20]; this may be because the extent of binder formation is relatively low in these pastes [24], so the chemical processes that induce shrinkage have not proceeded to the same extent as for a moderate modulus. It has been well known that the presence of a certain amount of silicate in the activator is beneficial to the formation of a dense microstructure, but too high a modulus, e.g. exceeding 1.5, tends to negatively affect the reaction rate [25,26]. The first reason is that a higher modulus means a lower pH due to the buffering effects of silanol deprotonation. Moreover, a silicate layer may form on the surface of the slag particles with excess SiO_2, hindering the further diffusion of ions. Less formation of reaction products leads to a coarser microstructure [27]. Hence, it is not optimal to have too much or too little SiO_2 in the activator, although the autogenous shrinkage can be lower.

Considering a fixed modulus of 1.5, the influence of w/b ratio and Na_2O content on autogenous shrinkage at 7 days is shown in Fig. 4. In general, the lower w/b ratio the higher autogenous shrinkage of AAS paste, the same as in PC systems [28]. This is related to the more severe self-desiccation due to the lower liquid content in the matrix. Compared to the effect of modulus, however, the effect of w/b ratio on autogenous shrinkage of AAS is minor. This indicates the important role played by silicate in the activator.

Fig. 5 plots the 7-day autogenous shrinkage results from the literatures on AAS paste, mortar and concrete with different mixture designs. The data points are categorized based on the type of activator. It appears that the autogenous shrinkage values of each AAS system vary in a big range. This reflects the complexity of AAS in terms of the number of adjustable parameters in the mix design. Unlike PC which is fundamentally controlled by the w/b ratio, the AAS system involves several chemical components in the reactions. Even for the same type of activator, different concentrations of chemicals can be used as demonstrated in Figs. 3 and 4. Moreover, the characteristics of the slag depend on the iron ore and production technology [32]. Globally speaking, the composition and reactivity of slags tend to differ between sources, although the characteristics of a slag from a particular source are generally highly consistent over time [33,34]. Additionally, the large variation in the autogenous shrinkage data should also relate to the different experimental protocols used in the literature; this will be discussed in more detail in Section 7.

Despite, a general trend can be observed in Fig. 5 that the autogenous

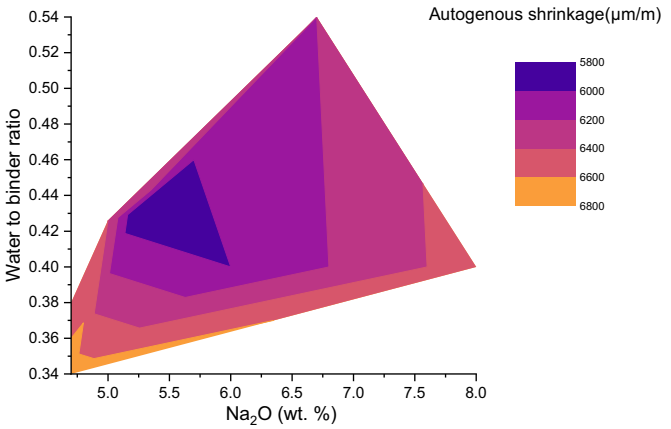

Fig. 4. Influences of w/b ratio and Na_2O content of the sodium silicate activator on the autogenous shrinkage of AAS pastes at 7 days with a constant modulus of 1.5 [22,29–31].

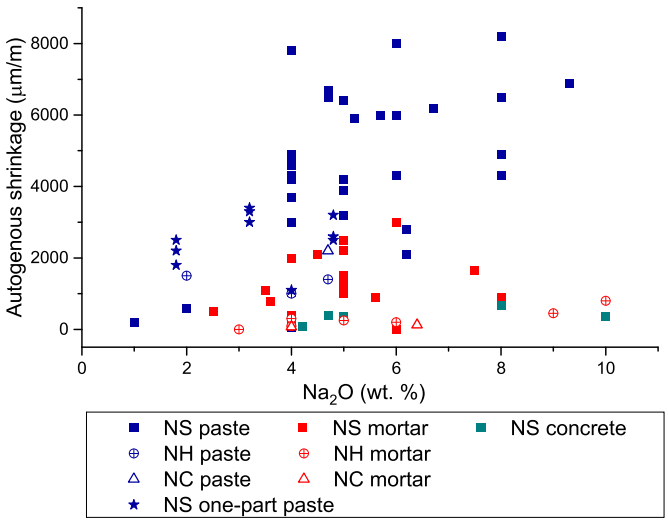

Fig. 5. 7-Day autogenous shrinkage of AAS paste, mortar and concrete with different mixtures designs. The data are categorized based on the type of activator. The data is from the references as summarized in Table A1.

shrinkage of sodium silicate-activated slag is higher than when other activators are used. It is also interesting to find that a conventional two-part sodium silicate-activated slag shows larger autogenous shrinkage than its one-part (just-add-water) counterpart. The reason behind this is probably the lower reaction rate and coarser pore structure of the latter system [35]. The effect of presence of aggregate in lowering the autogenous shrinkage is also clearly illustrated in Fig. 5 by separating the data points (marked in different colours) for AAS paste, mortar and concrete. This effect is due to the restrained shrinkage of the binder by aggregate, as also exists in PC-based mortar and concrete [36]. Moreover, the restraining effect of aggregates is more pronounced in AAS systems due to the presence of creep.

One may attribute the lower shrinkage magnitude of mortar and concrete than paste primarily to the dilution effect of binder by aggregate based on the fact that only the binder part shrinks. However, this is not true. Consider a paste (either PC or AAM) system showing a certain autogenous shrinkage (ε_{paste}). If part of the paste is replaced by voids, as shown in Fig. 6, the autogenous shrinkage of the new system ε'_{paste} would be approximately the same as ε_{paste}. Only if the voids are replaced by aggregates would the shrinkage be reduced. In other words, the lower shrinkage magnitude of concrete is not due to a lower binder content but the inclusion of aggregates which have high stiffness and do not shrink by themselves. The restraining effect of aggregate will be further discussed in Section 4.

Comparing the results in Fig. 5 and those for PC from the literature [9,28,37–39], we can see the autogenous shrinkage magnitude of AAS paste is generally larger than that of PC paste, which is normally below 2000 μm/m in the first month of curing. The same applies to mortar and concrete mixtures. An example comparison is shown in Fig. 7, after Cartwright et al. [40]. The autogenous shrinkage of the AAS mortar studied by those authors, using a sodium silicate activator, appears to be around 5 times as high as that of PC mortar with the same volumetric liquid/solid ratio. The mechanisms behind the generally higher autogenous shrinkage of AAS systems will be discussed in the next section.

3. Mechanisms

Dozens of studies have discussed the mechanisms of the autogenous shrinkage of AAS systems. As summarized in Fig. 8, several mechanisms or theories have been proposed. The majority of the literature agrees with the importance of capillary pressure/tension resulting from self-desiccation process, while other mechanisms may also co-exist rather

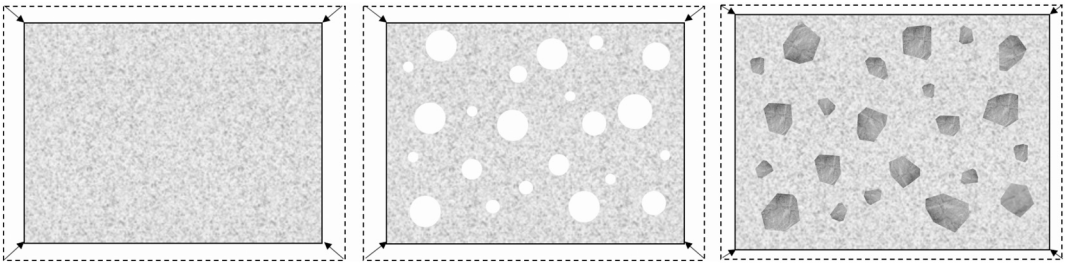

Fig. 6. Schematic diagrams of a paste, a paste with voids (paste′), and a concrete system. The paste contents of the latter two systems are the same. The order of autogenous shrinkage magnitudes among these systems would be $\varepsilon_{paste} \approx \varepsilon'_{paste} < \varepsilon_{concrete}$.

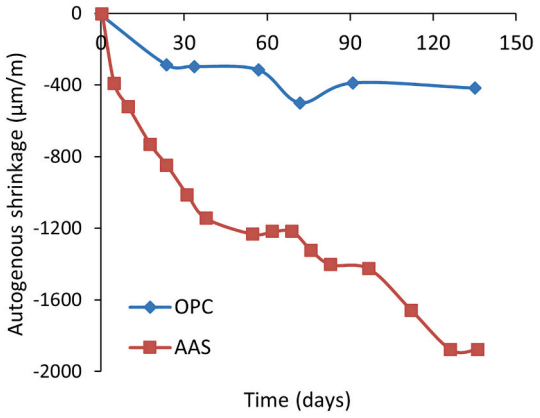

Fig. 7. Autogenous shrinkage of an AAS mortar with SiO_2/Na_2O of 1.22 and PC mortar with w/c ratio of 0.4, adapted from [40]. The two mixtures have the same volumetric liquid (water + activator)/solid (slag or cement) ratio of 1.30 and the same volume fraction of sand of 50.7 %.

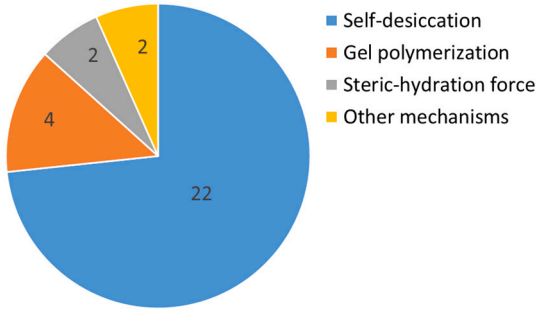

Fig. 8. Number of publications (till January 2023) where different mechanisms were proposed to explain the autogenous shrinkage of AAS: self-desiccation [21,24,40–59], polymerization/syneresis of C-A-S-H gel [22,60–62], steric-hydration force [63,64] and other unspecified mechanisms [65,66].

than be exclusive of each other.

3.1. Self-desiccation

3.1.1. Capillary pressure

The capillary pressure theory is evidenced by an extensive body of experimental results on chemical shrinkage [67,68] and drop in relative humidity (RH) [69]. The reasoning behind this theory is plausible. Similar to hydrated PC, AAS is a porous material, with the solid skeleton gradually hardening after casting and the liquid in the interstitial space being partially consumed (Fig. 9), leading to self-desiccation. Due to the reduction in absolute volume of the whole system (i.e. chemical shrinkage) and the hydrophilicity of the pore walls [52], the menisci,

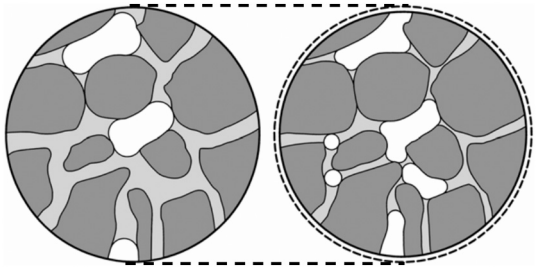

Fig. 9. Schematic representation of a cross-section of PC or AAS paste undergoing self-desiccation, from [16]. Left: low degree of reaction. Right: high degree of reaction. Solid matter (hydrate products and unreacted cementitious particles) is shown in dark grey; pore solution is light grey; and empty pore volume is white.

whose diameters gradually decrease, generate tensile stress which tends to reduce the distance between the solid surfaces. The resulting bulk shrinkage is the autogenous shrinkage. From this point of view, it is reasonable that capillary pressure should also be generated in AAS systems.[1]

However, doubt does exist regarding the time when this pressure starts to take effect. In hydrating PC, the onset time of capillary pressure is normally taken as the final setting time [9]. For AAS, however, the physically measured setting can occur much earlier than the start of acceleration period identified by calorimetry and the capillary pressure is reported to play an important role only after that [45,63]. This is probably because the stiffness of the matrix at final setting time, when the Vicat needle cannot penetrate, is not high enough yet to resist the building of menisci. Ma et al. [23] proved this point with direct measurements of internal stress in AAS pastes with a meniscus depression measuring system. According to that study, no significant internal capillary pressure developed in AAS around the final setting time. Chemical shrinkage might be the main reason for the autogenous shrinkage before the skeleton is stiff [58,70].

The amplitude of capillary pressure generated in AAS after the dormant period seems much larger than in PC. As indicated by the Laplace equation (Eq. (1)), the Kelvin equation (Eq. (2)), and their combination (Eq. (3)) [9], the capillary pressure is dependent on several factors, including the surface tension, the diameter of the meniscus, and the internal RH. For a partially saturated porous solid, the capillary pressure acts on the solid skeleton contacting with pore solution, therefore the effective force is also related to the saturation degree of the paste [71].

[1] This does not mean all AAMs are subjected to capillary pressure though. Alkali-activated metakaolin, for example, is found to show chemical and autogenous expansion in some stages [87,202,203], in which case the pore solution can be partially expelled so that menisci will not form.

$$\sigma = -\frac{2\gamma cos\theta}{r} \quad (1)$$

$$ln(RH_K) = \frac{2\gamma V_w cos\theta}{rRT} \quad (2)$$

$$\sigma = -\frac{ln(RH_K)RT}{V_w} \quad (3)$$

where σ (Pa) is the capillary pressure; γ (N/m) is the surface tension of the pore solution; r (m) is the radius of the menisci; RH_K is the internal RH due to meniscus formation; V_w (m^3/mol) is the molar volume of the pore solution; R (8.314 J/(mol·K)) is the ideal gas constant and T (K) is the absolute temperature.

According to the literature, AAS pastes have a high saturation degree [40], fine capillary pore structure (i.e. small diameter of menisci, especially for sodium-silicate-activated systems) [53,72] and a large surface tension of the pore solution due to the very high concentration of ions [46]. All of these factors contribute to a large drop in RH and a large capillary pressure. An example of the RH drop in an AAS paste, and corresponding generation of capillary pressure, is shown in Fig. 10. It is noted that the magnitude of the force in AAS varies for different mixtures, but is generally higher than in PC systems [55,73]. The large capillary force due to self-desiccation at least partially explains the large autogenous shrinkage of AAS.

3.1.2. Deformability

The autogenous shrinkage depends not only on the magnitude of the driving force but also on the deformability of the material. The elastic autogenous shrinkage of a paste induced by capillary pressure can be calculated as shown in Eq. (4) [71].

$$\varepsilon_{elas} = \frac{S\sigma}{3}\left(\frac{1}{K} - \frac{1}{K_S}\right) \quad (4)$$

where S (m^3 liquid/m^3 pore) is the saturation fraction; σ (Pa) is the capillary pressure; K (Pa) is the bulk modulus of the paste; and K_S (Pa) is the bulk modulus of the solid skeleton.

It can be seen from Eq. (4) that the elastic deformation is negatively correlated with the bulk modulus of the paste, which depends in turn on the elastic modulus E (Pa) and Poisson's ratio υ of the material (Eq. (5)).

$$K = \frac{E}{3(1-2\upsilon)} \quad (5)$$

At very early age, e.g. before the acceleration period, the elastic modulus of AAS has been reported to remains <1 GPa [63], with no apparent change around the point of final setting as measured by Vicat needle method. The deformability of the material is therefore high, and the chemical shrinkage can fully convert into autogenous shrinkage [58]. During the acceleration period, the elastic modulus of AAS increases [63]. Nonetheless, the elastic modulus of hardened AAS is still measured to be lower than that of PC with similar compressive strength, at both paste and concrete scales [9,63,74–76]. This means that there will be a larger deformation in AAS under the same magnitude of driving force.

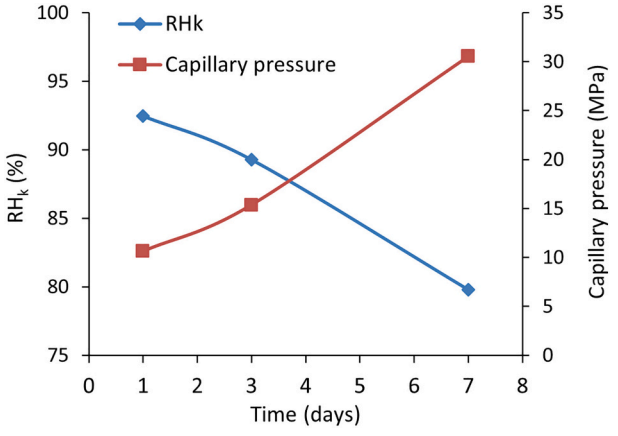

Fig. 10. RH_k drop and capillary pressure in an AAS paste with SiO_2/Na_2O of 1.5 and w/b of 0.38 (data from [63]).

Moreover, it is noted that binder materials are not purely elastic, especially for AAS which is found to have pronounced viscoelasticity, partially due to the structural incorporation of alkali cations that reduces the stacking regularity of C-A-S-H layers and makes the gel prone to collapse and slide (Fig. 11) [55,61]. As simulated in [55,63], the time-dependent or creep deformation under internal force accounts for a larger contribution than the elastic deformation in the total autogenous shrinkage of AAS paste. Both the early-age and late-age creep coefficients of AAS are reported to be higher than those of PC with and without SCMs [9,63,77–80]. The pronounced deformability contributes even more than the high capillary pressure to the much larger autogenous shrinkage of AAS systems compared to PC.

It is worth noting that the viscoelasticity of the reaction products affects not only the shrinkage but also other engineering properties of AAS. For example, for restrained AAS, the local viscoelastic deformation can cause stress relaxation, as will be further discussed in Section 5. The bonding between concrete and reinforcement may also be influenced. For prestressed members, in particular, the viscoelasticity of concrete can lead to prestress loss and long-term deflection [82,83]. These effects should be taken into account when using AAS concrete in structures.

3.2. Other driving forces

Without denying the existence of capillary pressure, various researchers have proposed that other driving forces also play roles in the autogenous shrinkage of AAS, as they found that the capillary pressure theory alone could not completely explain the observed behaviour. Evidence was provided from different aspects. For example, Kalina et al. [65] used an amino alcohol-based shrinkage reducing admixture (SRA) which can reduce the surface tension of the pore solution of AAS paste, but the autogenous shrinkage was only affected minimally. Fang et al. [66] found different shrinkage magnitudes of AAS with partial fly ash substitution on the first day while the drops in internal RH of these mixtures were similar. One may argue that the discrepancy can be due to the presence of fly ash, which brings differences in the chemistry of reaction products. However, according to [63,84], the incorporation of fly ash does not change intrinsically the nature of reaction products, i.e. C-A-S-H type gels, when a considerable amount of slag is present. Li et al. applied both internal curing [29] and external curing [63] to eliminate the inner desiccation of AAS, but considerable autogenous shrinkage was still observed in both cases, especially at the first dozens of hours. These results indicate that self-desiccation may not be the exclusive mechanism of the autogenous shrinkage of AAS.

Alternatively, Uppalapati [62] proposed that the continuous poly-condensation reaction between two adjacent gel units also contributes to the autogenous shrinkage of AAS. This reaction happens mainly in the dormant period when the solid network is being formed and the distance between solid particles becomes shorter as a result [62]. This hypothesis is in line with the finding of Chen et al. [22], who stated that the spontaneous syneresis of C-A-S-H gels is responsible for a large part of the autogenous shrinkage of AAS pastes, especially those prepared with a high silicate modulus. Furthermore, Zheng et al. [60] explained the autogenous shrinkage of AAS by an increased polymerization degree of Si between C-A-S-H gels. Although different terms (poly-condensation, Si polymerization, and syneresis) were used in these studies, similar phenomena were described, as demonstrated in Fig. 12.

In fact, the polymerization between silicates associated with dehydration occurs not only in AAS but also in fly ash and metakaolin-based geopolymers [86,87]. The early-age autogenous shrinkage of alkali-

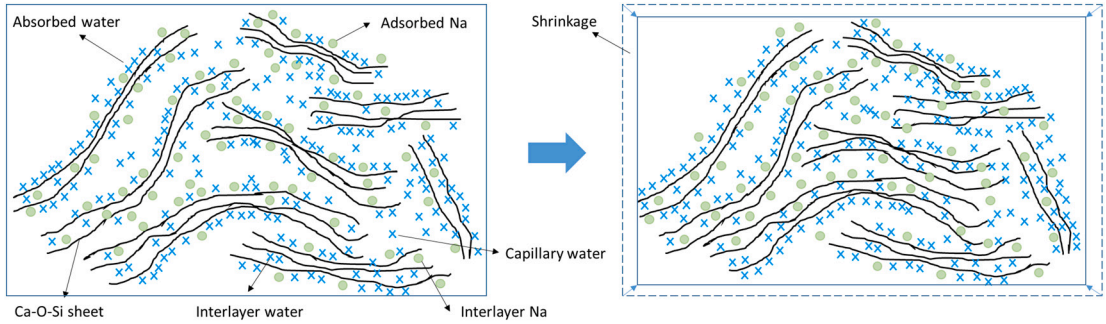

Fig. 11. Illustration of deformation of C-A-S-H gel under internal driving force, e.g. capillary pressure, adapted from [61]. Partially due to the incorporation of Na [81], the gel is more prone than C-S-H gel to collapse and slide [61], leading to viscoelastic deformation, part of which is unrecoverable.

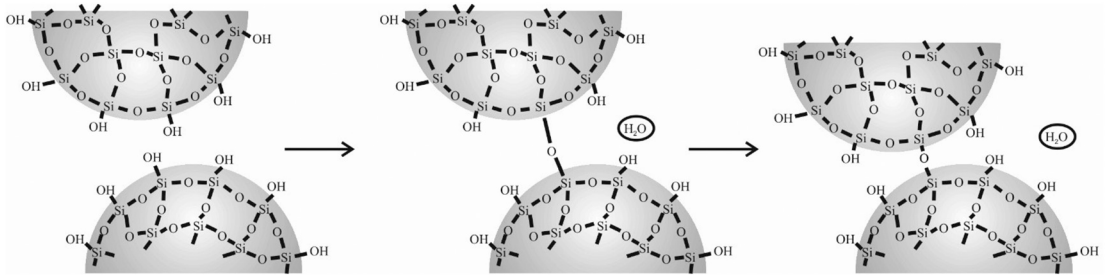

Fig. 12. A schematic diagram of shrinkage caused by polymerization/syneresis of silicate particles, from [85]. Constituents other than silicate and hydroxide groups are omitted for clarity.

activated fly ash was largely attributed to this process according to [88]. By the polymerization theory, the autogenous shrinkage of AAMs is actually explained from a gel or even molecular level. This explanation of dimensional change driven by chemical reactions does not invoke micro- or macro-scale physical forces, like capillary pressure [89], and so may be valid only for early-age low-calcium AAMs that do not self-desiccate. It is less likely to be able to provide a full description of the behaviour of AAS by neglecting the physical processes, especially after the very early age.

The conversion of silicates in the pore solution from free ions to a connected solid network is expected to play an important role in polymerization-induced shrinkage. It is thus reasonable to find that the bulk shrinkage caused by gel polymerization happens mainly during the hardening process [22,60,62]. Within a hardened and stable binder structure, the positions of the gel particles are "fixed" by adjacent gel, hence no longer mobile. However, it should be noted that the hardening of AAS as described here, based on gel interconnectivity, can be to some extent different from the definition of final setting as determined by the Vicat test. Due to the formation of initial gel products, AAS paste can gain yield stress sufficiently rapidly so as to resist the penetration of the

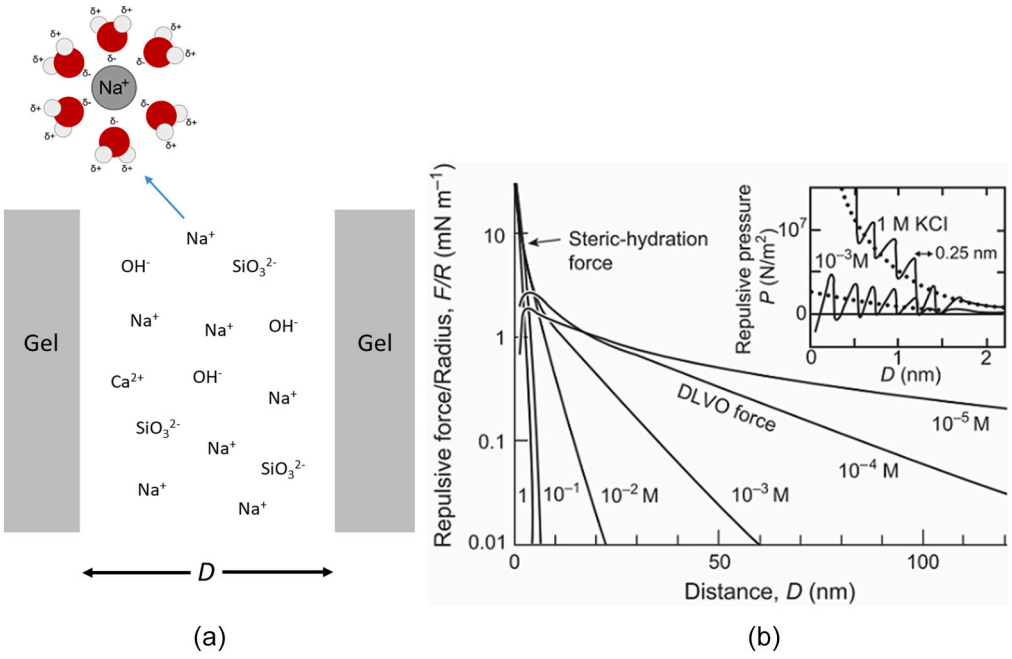

Fig. 13. (a) Schematic representation of the ions and hydration shells between gel particles in AAS, adapted from [95]. (b) An example of steric-hydration force in comparison with DLVO force, after [91]. The forces were measured between curved mica surfaces in KNO_3 or KCl solutions (qualitatively similar results are obtained in other electrolyte solutions). At 10^{-5} and 10^{-4} M the force follows the theoretical DLVO force law at all separations. At 10^{-3} M and higher concentrations more cations adsorb (bind) onto the surfaces and bring with them their water of hydration. This gives rise to an additional short-range hydration force below 3–4 nm (see inset for details).

Vicat needle, but a stable structure may not yet form [63,90].

While the explanation of autogenous shrinkage of AAS by gel polymerization is to some degree plausible, key issues exist with regard to the lack of direct experimental proof and the difficulty to quantify the corresponding shrinkage. The same issues were encountered by the proposition of steric-hydration force by Li et al. [63,64], as they found that the autogenous shrinkage of AAS develops rapidly in the acceleration period when the drop in internal RH was limited. They attributed part of the early-age autogenous shrinkage to the reduction of steric-hydration force. In electrolytic solution, e.g. the interstitial solution, ions (especially divalent ions) would absorb neighbouring water molecules to form hydration shells and the counter overlap of the shells of individual ions would provide strong repulsive steric force to avoid the solid surfaces reaching closer (Fig. 13a) [91]. As reported in [92,93], the repulsive steric-hydration force is stronger than DLVO (Derjaguin-Landau-Verwey-Overbeek) forces and increases with the increase of concentration of ions, as illustrated in Fig. 13.b. During the acceleration period, the ion concentrations of the pore solution decrease dramatically [94], so that the repulsive force due to the steric effect of hydration shells also decreases. Meanwhile, the attractive forces between gel particles remain, and hence bulk shrinkage is generated. This type of force has been assumed to take effect only in fine gel pores (<4 nm) when the chemical environment in the system is rapidly changing [63]. On that scale, it is difficult to define whether the deformation taking place is elastic or plastic. Atomic force microscopy (AFM) might be a useful tool for future studies to provide evidence on the influence of ion concentrations on the interaction between gel particles immersed in a solution.

Apart from shrinkage, AAS seems also to have the potential to expand possibly due to the formation of crystalline reaction products such as hydrotalcite-group minerals [96,97]. However, the amount of these crystals is normally limited in AAS [98] and the formation of them is not as expansive as ettringite in PC systems [99,100]. Hence, the expansion associated with their formation can only compensate for part of the autogenous shrinkage in a certain stage [101–103]. Currently, no method is available to quantify this effect in AAS.

In summary, there is at least one consensus that has been reached in the literature: the capillary pressure resulting from self-desiccation should be an important driving force of the autogenous shrinkage of AAS. Due to the large surface tension of the pore solution, dense pore structure, and high saturation degree of AAS, the magnitude of capillary pressure is much higher than that in Portland-based cementitious materials. The deformability of AAS under the capillary pressure is also large due to the pronounced viscoelasticity of the C-A-S-H gels. However, the self-desiccation theory cannot fully explain the autogenous shrinkage of AAS. While capillary pressure plays a major role in micro-scale after a stable microstructure is formed (as in PC systems), alternative theories, e.g. poly-condensation and steric-hydration force, provide insights into the forces between gel particles at very early age. These theories are proposed specially for AAMs, where different chemistry from the cement hydration is involved. However, due to the lack of quantitative evidence from experiments, these theories remain as hypotheses until now.

4. Modelling and prediction

Modelling of autogenous shrinkage is significant for shrinkage prediction and standardization of AAS, and different modelling approaches have been used in previous studies. An intuitive approach is to apply the available models developed for PC-based materials. Ma and Dehn [50] used the models defined in the JSCE Specification for Concrete Structure 2007 [104] and in the *fib* Model Code 2010 [105] to calculate the autogenous shrinkage of AAS concrete and found that neither of them gave a good estimation, neither in total shrinkage magnitude nor in terms of time-dependency (Fig. 14). The increase of the measured autogenous shrinkage after 28 days is much more significant than

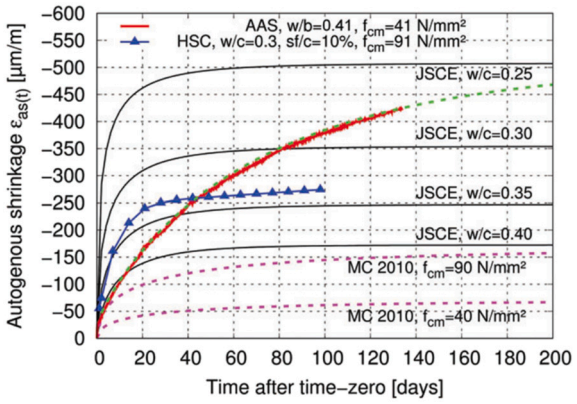

Fig. 14. Autogenous shrinkage of an AAS concrete in comparison with a high-strength PC concrete (HSC), from [50]. Models in the JSCE Specification 2007 and the *fib* MC 2010 were used for calculation.

predicted by the codes. This result is consistent with observations in [106], where the autogenous shrinkage of AAS mortar was found not to have stabilized even at an age of 100 days. Li et al. [30] also applied the *fib* Model Code to simulate the autogenous shrinkage of AAS concrete and found significant underestimation, too.

One reason for these discrepancies lies in the fact that the empirical parameters involved in the model codes were defined based on a vast of experimental data on compressive strength and autogenous shrinkage of PC-based concretes. For AAS, the mechanisms controlling microstructure development and shrinkage are different from those which govern PC behaviour, and the driving force for shrinkage is much larger, as discussed in Section 3. Thus, the models developed for PC will generally underestimate the autogenous shrinkage of AAS, unless using deliberately reduced w/b ratios.[2] Another reason should be the different reaction kinetics of AAS and PC. The early-age reaction rate and development of microstructural maturity of AAS may not be as high as that of PC, in spite of the high early-age strengths that can be achieved by AAS [19,107,108]. Part of the reason is the formation of the product rims surrounding the unreacted slag grains, which hinders further diffusion of ions at early age. With the elapse of time, the reaction in AAS keeps proceeding and the gain in strength of AAS can be considerable even after 28 days [75,109]. Along with the further reaction, the self-desiccation process which is a main shrinkage mechanism in AAS also develops. The pronounced viscoelasticity of the AAS material also means that the deformation will keep increasing even under a stable force. Therefore, an autogenous shrinkage model that reaches a plateau in a short period, as predicted by some empirical models for PC, will not fit the time-dependent behaviour of AAS.

Compared to compressive strength, degree of reaction (DoR) seems a more appropriate parameter to reflect the early-age evolution of autogenous shrinkage of AAS. According to [110], the autogenous shrinkage of alkali-activated slag and fly ash pastes correlates linearly with the reaction heat, which is normally assumed to be proportional to the DoR. Abate et al. [55] studied different AAS mixtures and also identified linear relationships between the autogenous shrinkage and DoR depending on the activator dose. However, irrespective of the activator composition, they observed that the autogenous shrinkage of AAS mixtures was much higher than that of PC at a similar DoR [55], which is consistent with the findings discussed in Section 2.

Despite the linear relationship that has been identified between autogenous shrinkage and DoR of AAS, the existing body of

[2] Nonetheless, according to [201], when the 28-day autogenous shrinkage of AAS is known and used as the input, the mathematical function in Eurocode2 is able to estimate the autogenous shrinkage at other ages.

experimental data is not yet sufficient to establish empirical models that can predict the autogenous shrinkage of AAS. One approach that can quantify the autogenous shrinkage is based on poromechanics, derived from Hooke's law. As shown in Eq. (4), the elastic deformation of PC or AAS paste can be calculated from the saturation degree, capillary pressure and bulk modulus of the material. It was found in [22] that the autogenous shrinkage of AAS paste increases almost linearly with the capillary pressure, while the influence of elastic modulus is marginal. Internal RH is a key parameter that can be used in estimating the capillary pressure (Eq. (3)). As reported in [55], the relationship between RH and the autogenous shrinkage of the specimens is linear except at early age. This finding is in line with the results of [111].

With the experimentally measured RH, elastic modulus and saturation degree as inputs, Li et al. [63] calculated the elastic deformation of AAS paste under capillary pressure, and found that it accounts for only <25 % of the total autogenous shrinkage. Very similar proportions of elastic deformation were identified by Abate et al. [55]. These studies proved quantitatively that non-elastic deformation (creep) must also be considered in predicting the autogenous shrinkage of AAS. In order to do that, Li et al. [63] used an empirical equation to obtain the creep coefficient based on DoR and w/b ratio, summing the increments of creep taking place in each time interval to calculate the total deformation (Fig. 15). As an alternative approach, Abate et al. [55] applied a spring-dashpot model to simulate the creep compliance of AAS paste (Fig. 16). Both of these approaches have been shown to result in good predictions of the autogenous shrinkage of AAS pastes.

However, these two approaches show a common drawback, which is the oversimplification of parameters. Due to the insufficient database available to elaborate the behaviour of AAMs, some input parameters in these models were estimated empirically to simplify the mechanical compliance of the maturing AAS, without fully describing the microscopic phenomena occurring in the paste, such as hydrate growth, concentration changes in pore solution, and microcracking [55]. Furthermore, the possible existence of other driving forces than capillary tension was not considered in these models. Nonetheless, using numerical models with some empirical parameters seems to be a feasible way to predict the autogenous shrinkage of AAS at present, while researchers continue in parallel to build a comprehensive database for various AAS mixtures. To achieve this, extensive experimental effort will be required in order to establish chemistry-informed and microstructure-informed models.

Based on the calculated or measured autogenous shrinkage of AAS paste, the autogenous shrinkage of AAS mortar and concrete can be predicted by considering the inclusion of aggregates (as discussed in Section 2, the effect of aggregate is not simply diluting the binder) and

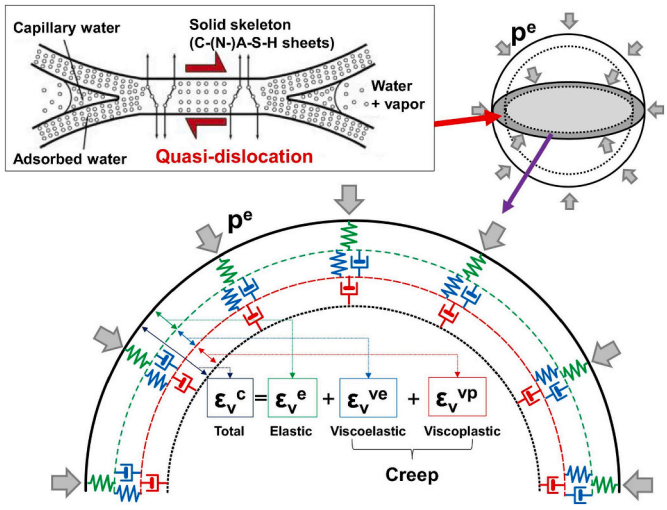

Fig. 16. Schematic representation of the model used in [55] to simulate the creep compliance of AAS paste.
The figure is from [55].

their interactions with the pastes within a composite material. For PC-based systems, composite models including Pickett's model [112], Hobbs' model [113], Tazawa's model [114], and others, generally based on classic mechanics, have been shown to provide satisfactory predictions of autogenous shrinkage [78]. For AAS systems, however, these models appear not to be directly applicable [30]. A key reason is believed to be the lack of inclusion of creep phenomena in these composite models. It is well known that the deformation of paste is restrained by aggregates, so that the shrinkage of concrete is always lower than that of corresponding paste. However, the stiff aggregates can more effectively restrain the viscous deformation than the elastic deformation of the paste [36]. Therefore, assuming the deformation to be solely elastic would lead to underestimation of the restraining effect of aggregates, thus overestimating the shrinkage of concrete.

To consider the effects of creep, researchers have used the concept of "effective" or reduced elastic modulus of the paste, or increased elastic modulus of the aggregates [36]. Either way, a better estimation can be reached in a practical sense. However, choosing a reduced elastic modulus of the paste, e.g. 1/3 of the measured value as suggested by [115], is somewhat arbitrary and lacks strict theoretical underpinnings. Additionally, a constant value of elastic modulus, even though reduced from the value for the paste alone, cannot properly reflect the time-

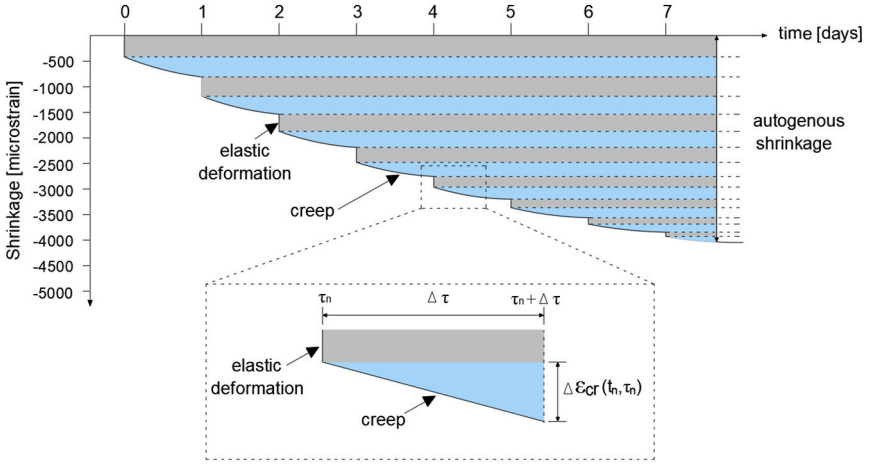

Fig. 15. Schematic representation of the model used in [63] to simulate the creep compliance of AAS paste.
The figure is from [63].

dependent characteristics. To consider the changing elastic modulus and creep of AAS paste with time, Li et al. [30] extended Pickett's model [112] by separately calculating the elastic and non-elastic deformations of the paste, and updating the force between paste and aggregate after each time step. By use of this extended Pickett's model, the autogenous shrinkage of AAS concrete was predicted accurately (Fig. 17).

Nonetheless, a limitation of Pickett's model, in both original and extended forms, is the assumption that the aggregate particles are much smaller than the surrounding paste, and that the restraining effects of each particle are independent of each other. In real concrete, the volume fraction of aggregates is considerable, and the stress fields generated in the paste due to the presence of multiple aggregates will inevitably overlap. Future research efforts are definitely needed to develop more realistic models capable of taking into account complex force fields. Finite element modelling (FEM) might be useful for this purpose [116], but few studies can be found using this approach for shrinkage of AAS systems. A possible challenge in using FEM is to assign a viscoelastic constitution to the discrete beams of the mesh [117].

5. Cracking tendency

Restrained shrinkage can lead to tensile stresses which may induce cracking of the material. The cracking tendency of building materials is a more crucial criterion for the serviceability evaluation than the magnitude of free shrinkage [118,119]. Cracks can cause a series of problems with regard to mechanical properties, durability, and aesthetics (see Fig. 1) [120]. As was shown in Section 2, AAS systems show high autogenous shrinkage, but we cannot immediately conclude that they must also run a high cracking risk under restrained conditions, since the occurrence of cracking is determined by multiple factors, including shrinkage, elastic modulus, tensile strength, creep and relaxation [121]. To date, not many studies have evaluated the cracking tendency of AAS. The experimental methods used by researchers include mainly ring tests and the temperature stress measuring machine (TSTM) test (Fig. 18), in which annular and dog-bone shaped specimens were restrained, respectively.

Compared with PC concrete with similar strength, the cracking proneness of AAS concrete is not necessarily higher in spite of its larger autogenous shrinkage [124]. The key reason is attributed to the pronounced viscoelasticity of the material (as discussed in Section 3.1.2), which results in greater relaxation of the induced tensile stresses. The

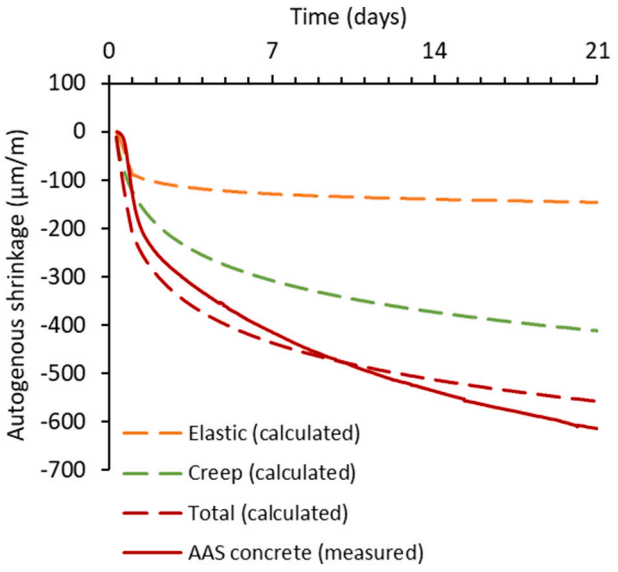

Fig. 17. Calculated autogenous shrinkage of an AAS concrete according to the extended Pickett's model (dashed lines) in comparison with the measured autogenous shrinkage (solid lines), adapted from [30].

significant role of relaxation in the stress evolution in AAS systems has been emphasized in several studies [124–126]. Modelling approaches have been proposed to estimate the internal stresses by considering the elastic part of autogenous shrinkage, elastic modulus, relaxation, and tensile strength of the material. The elastic part of autogenous shrinkage can be estimated either based on the driving force of autogenous shrinkage, e.g. capillary pressure, and the elastic modulus [63], or from the total deformation with deduction of creep [124,126]. Qualitatively speaking, aside from the complexity of these approaches, the cracking tendency of restrained AAS increases with the generation of internal stress, e.g. capillary pressure, and decreases with the extensibility of the material [118].

The presence of aggregates is essential in defining cracking tendency in mortars and concretes. Li et al. [29] investigated the cracking tendency of sodium-silicate activated slag paste with a ring test (the diameter and the height of the concrete ring were smaller than specified in ASTM C1581 [122] for concrete). Without aggregate, AAS paste shows cracking within 14 h after casting. The tensile stress generated by the restrained autogenous shrinkage was close to zero in the first hours. This corresponds to the low stiffness of this material in this period as discussed in Section 3.1.2. During the acceleration period, the tensile stress increased rapidly, exceeding 2 MPa and leading to sudden cracking [29]. The partial replacement of slag by fly ash can reduce the autogenous shrinkage and also the cracking tendency of AAS pastes, according to [49]. However, cracking still occurred within 60 h.

Uppalapati [62] evaluated the cracking tendency of sodium-silicate activated slag and fly ash mortars with ring test and observed similar cracking times. By contrast, the incorporation of sodium carbonate and sodium sulfate in the activator significantly prolonged the onset time of cracking, and decreasing the alkalinity of the activator further delays cracking. Nonetheless, the cumulative heats of these mortar mixtures at the time of cracking were observed to be rather similar [62]. This indicates that the reaction kinetics might be a key factor determining the cracking tendency of AAS. Support for this point is found in [75], where the mechanical properties and cracking tendencies of AAS and PC-based concretes with similar strengths were compared. While AAS concrete showed higher autogenous shrinkage, its cracking time was later than CEM I, CEM III/A, and CEM III/B concretes. However, the DoR of these mixtures at cracking time, defined by the ratio between corresponding reaction heat and ultimate reaction heat, was similar as shown in Fig. 19 [75]. These results may indicate the possible use of DoR as an index to evaluate the cracking tendencies of AAS-based mixtures. Nonetheless, doubt exists regarding whether the reaction heat obtained by calorimeter can be used to estimate the real reaction degree of different mixtures. The physicochemical mechanism behind the strong correlation between DoR and cracking time of AAS and PC-based concretes identified in [75] has not been clarified yet.

The potential correlation between DoR and occurrence of cracking of AAS systems indicates that attempts to lower the cracking tendency of these materials by elevated-temperature curing may not be effective, since it will accelerate the reaction [62]. Under that circumstance, both the rates of autogenous shrinkage and the mechanical properties at early age will be increased. The results of the ensuing competition between shrinkage-induced stress and tensile strength are unclear, but would be expected to depend on the details of binder microstructural development based on chemistry and other characteristics. The additions of superabsorbent polymer (SAP) or fibres, which target reduction of the internal stresses or an increase in the tensile strength, respectively, are more effective in reducing the cracking tendency of AAS paste and concrete [124,127]. The influence of SAP on the autogenous shrinkage of AAS will be elaborated in the next section.

While the occurrence of thorough cracking of AAS paste or concrete can be identified easily through the sudden drop in internal stress, the development of microcracking is harder to detect. Unlike the drying-shrinkage-induced microcracks that can be observed on the surfaces of the specimens [128–130], autogenous-shrinkage-induced microcracks

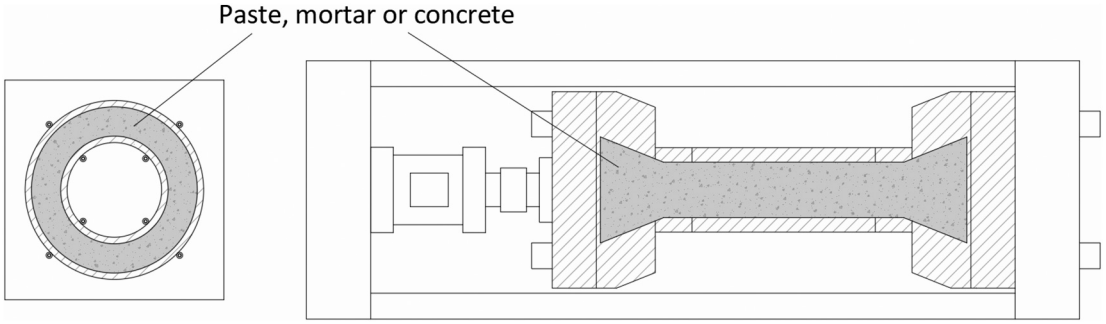

Fig. 18. Schematic representations of ring test and TSTM, adapted from [122,123], respectively. The specimens have an annular and dog-bone shape, respectively.

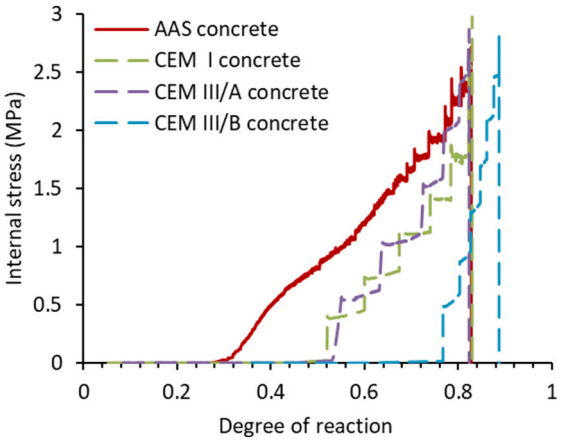

Fig. 19. Autogenous shrinkage-induced stress in AAS and PC-based concretes as a function of DoR, adapted from [75]. The DoR was defined as the ratio between the reaction heats at a certain age to the ultimate reaction heat which was determined by extrapolation of the experimentally measured reaction heat.

can form inside the matrix, for example, perpendicular to the interface with non-shrinking phases including aggregates and unreacted particles [30]. AAS systems, which have larger autogenous shrinkage, seem to suffer more from microcracking than PC-based systems [131]. The development of microcracking is believed to be related to the visco-elasticity of the reaction products [30]. It has been discussed that the C-A-S-H gel in AAS has higher viscosity and the local creep contributes to stress relaxation to delay the failure of concrete. However, the relief of stress in highly stressed zones through local creep is likely to cause new stress concentrations in other zones [123]. In other words, the reduced risk of thorough cracking of AAS by viscous deformation of gels is expected to come at the cost of the development of microcracking.

Microcracking has been regarded as responsible for many unwanted phenomena in AAS, such as the observed scatter (and even reductions) in elastic modulus [75,132] and flexural/tensile strength [24,131], the fact that tensile strength-to-compressive strength ratios are sometimes unexpectedly low [75], and even carbonation [133]. These hypotheses appear plausible since no reduction in compressive strength was observed in parallel with the loss of other mechanical properties, which is to say, the unstable tensile strength and elastic modulus were not because of a uniformly weakened matrix. Under drying conditions, the development of microcracks would be enhanced. Unlike autogenous shrinkage that occurs homogenously in the paste, drying shrinkage is heterogeneous and its magnitude depends on environment humidity and properties of the material such as pore structure, stiffness, size and shape, etc. In the surface regions, autogenous shrinkage and drying shrinkage are combined. This coupled with the possible effect of carbonation can lead to propagation of microcracks into visible cracks, which will further impair the durability of the concrete. The issue of shrinkage-induced cracking certainly warrants further research attention in the future.

Direct evidence of microcracking caused by autogenous shrinkage has not been intensively reported. Although scanning electron microscopy (SEM) has been used to observe cracks in AAS [47,56,134,135], the sample preparation normally involves cutting and/or crushing to get pieced samples and drying and/or freezing to stop the reaction [108]. These procedures can all result in microcracking of the sample. Therefore, it is not easy to conclude that any observed microcracks originate specifically from the autogenous shrinkage. Non-destructive testing methods, e.g. nano-computed tomography (CT) [136,137], may be better alternatives for this task, but also raise non-trivial questions around sample preparation and imaging protocols. Wu [14] used optimal microscope to observe the autogenous shrinkage-induced microcracking in AAS mortar (Fig. 20). The sample was impregnated with epoxy immediately after sealed curing, so that the effect of drying was eliminated. Microcracks were found to mainly develop in the region surrounding sand particles and the crack width was mostly smaller than 30 μm. More research is required to gain clear profile of microcracking in order to evaluate the effect of autogenous shrinkage on mechanical properties and durability of AAS systems.

6. Mitigation

Due to the potentially severe consequences of autogenous shrinkage of AAS systems, it is necessary to identify suitable shrinkage-mitigating strategies. The strategies that have been realized in the literature are mainly based on incorporating additives or admixtures into the system, such as surfactants, expansive admixtures, nanoparticles, internal curing

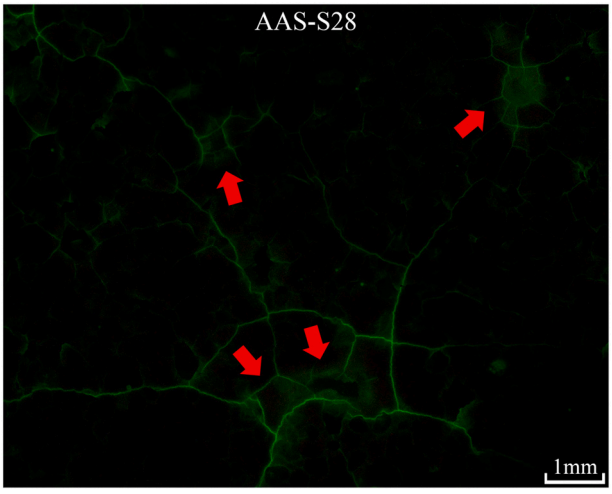

Fig. 20. Microcracks in AAS mortar after sealed curing for 28 days, observed by optical microscope with fluorescence and filter [14]. The arrows indicate the positions of sand particles located beneath the observed surface.

agents, or metakaolin. Elevated temperature curing was also used for this purpose.

6.1. Surfactants and other chemical admixtures

Surfactants can reduce the surface tension of the pore solution, so that they can reduce the capillary pressure caused by self-desiccation (see Eq. (1)) [138]. Many shrinkage-reducing admixtures (SRAs), superplasticizers and air-entraining agents are based on surfactants [139] and have been widely used to reduce the shrinkage of cementitious materials [140].

For AAS, Hu et al. [141] reported that a commercial SRA that described as "oxyalkylene alcohol-based" could significantly reduce the autogenous shrinkage, irrespective of the modulus of the sodium silicate activator. A polypropylene glycol-based SRA was also found to be effective in mitigating the autogenous shrinkage of AAS without decreasing strength [142,143]. Kumarappa et al. [46] found that an SRA could reduce the autogenous shrinkage by 75 % when applied at a dosage of 7.5 % relative to the mass of slag (although the dosage seems very high to the authors' opinion). However, some SRAs show side effects when applied in AAS, such as hexylene glycol, which leads to strength loss [144]. Bakharev et al. [145] found that an alkyl aryl sulfonate was effective in mitigating the autogenous shrinkage of AAS concrete. Although the early age strength of the specimens became lower with this admixture, the strength at 28 days was not significantly influenced.

Palacios and Puertas [146] studied the influence of four types of superplasticizers (based on polycarboxylates, vinyl copolymers, melamine and naphthalene) on the properties of AAS and found that all admixtures except the naphthalene-based product lost their fluidifying properties in the alkaline media. The naphthalene-based superplasticizer was reported to even increase the autogenous shrinkage of AAS concrete [145], although it can retain its chemical structure in strong alkali environments. With the same aim of lowering the surface tension of the pore solution, cooking oil was found by Huang et al. [44] to show a more pronounced shrinkage-mitigating effect than a conventional SRA. Although the 7-day compressive strength was reduced, the 28-day compressive strength of AAS concrete was almost the same as that of the reference mixture.

Besides surface tension, the contact angle of the pore fluid on the pore wall also determines the magnitude of capillary pressure (see Eq. (1)). For hydrophilic materials like cement and slag, the contact angle of water is normally taken as zero [16,147], in which case the Kelvin radius is equal to the pore radius. By adding a type of biofilm into slag, Qu et al. [52] increased the hydrophobicity of AAS and thus increased the contact angle between pore solution and pore wall. The capillary pressure was therefore reduced at a given pore radius, and so was the autogenous shrinkage.

6.2. Expansive admixtures

Hu et al. [141] added MgO into AAS mortars and found that the expansion effect was not as significant as found for comparable PC-based systems. A similar conclusion was drawn by Yang et al. [148]. The reason was attributed to the dense structure of AAS so that MgO had less access to water to form $Mg(OH)_2$. Instead, it formed M-S-H or hydrotalcite-like phases, with lower associated volume increase. In contrast, the results of Li et al. [149] showed that MgO can reduce the shrinkage of alkali-activated slag blended with fly ash, with an improvement in early age strength. Their results were confirmed by Yang et al. [150], who found that the addition of reactive MgO can mitigate both the autogenous shrinkage and the drying shrinkage of similar mixtures. However, for sodium carbonate and sodium sulfate-activated slag systems, the addition of MgO can increase the autogenous shrinkage [59].

Gypsum may also act as an expansive agent. It was found that the incorporation of gypsum coarsened the pore structure of AAS and triggered the formation of expansive sulfate-rich phases (e.g. ettringite) [101]. The shrinkage was therefore partially compensated, as consistent with the results obtained by Bakharev et al. [145]. However, the early-age expansion was insufficient to offset the subsequent long-term shrinkage, as reported by Ye and Radlińska [101].

The addition of CaO was also not effective in reducing the shrinkage of AAS [101]. The reasons given by the authors of that study were the refined pore structure and lack of a reduction in chemical shrinkage. In addition, CaO can rapidly release Ca^{2+} after contacting the activator and further accelerate the setting of AAS, that is already sometimes faster than desired. $Ca(OH)_2$ seems to enhance the autogenous shrinkage at very early age, too, due to the increased alkalinity and facilitated reaction rate according to Zhu et al. [96]. After the first days, however, adding $Ca(OH)_2$ can successfully mitigate the autogenous shrinkage of AAS (Fig. 21). The mechanism behind this lies in the coarsened mesopores and increased elastic modulus [96]. In addition, the formation of expansive crystals such as C_2ASH_8 and C_4AH_{13} also contributes to the shrinkage mitigation.

6.3. Nanoparticles and pore modification

Liu et al. [134] added nanosized C-A-S-H gel particles into AAS mortar, and found that the autogenous shrinkage could be reduced by >20 %. The reduction of autogenous shrinkage was explained by the reduced overall porosity and the increased proportion of meso-pores in the AAS mortar [134]. This explanation was opposite to the findings of Yang et al. [151], who attributed the reduced autogenous shrinkage of AAS paste with added nano-TiO_2 to the reduced overall porosity and a smaller volume proportion of mesopores.

In fact, the volume fraction of mesopores is not likely to be the sole factor that influences the capillary pressure and the autogenous shrinkage. The diameter of menisci is determined not only by the pore size distribution, but also by the volume that is emptied due to chemical shrinkage, i.e. the degree of saturation [152]. A larger saturation degree and a coarser pore structure would lead to larger menisci (see Fig. 9) and consequently a lower capillary pressure. Furthermore, the pore size distribution also influences the elastic modulus of the paste, which provides resistance to the shrinkage. Therefore, more factors including chemical shrinkage, pore size distribution, degree of saturation, and elastic modulus, need to be considered when predicting the mitigating effect on autogenous shrinkage.

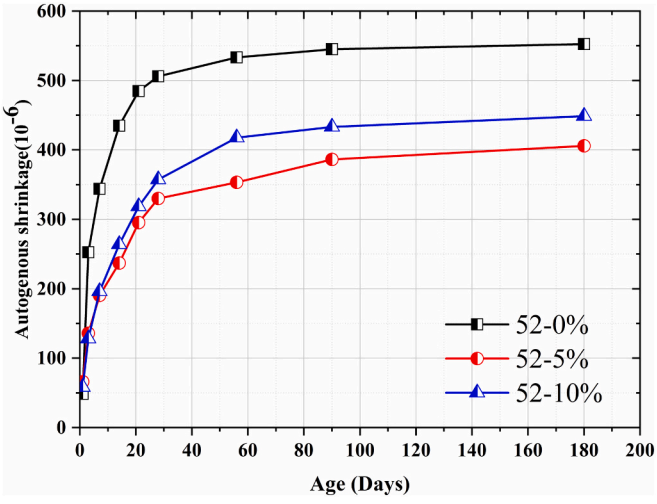

Fig. 21. Autogenous shrinkage of AAS concrete (w/b = 0.52) with different dosages (0 %, 5 % and 10 %) of $Ca(OH)_2$.
The data is from [96].

6.4. Internal curing agents

Internal curing is normally realized by adding SAP or lightweight aggregate (LWA) (e.g. pumice or expanded clay) into a binder or concrete [153–157]. SAPs or LWAs can act as liquid reservoirs for the system, providing extra liquid to compensate for the liquid consumption during hydration [154]. By internal curing, the intention is to mitigate the capillary pressure induced by self-desiccation.

Many studies have been conducted on SAP incorporation into AAS paste, mortar and concrete. The autogenous shrinkage of sodium silicate-activated slag can be reduced by more than half, while sodium hydroxide and sodium carbonate-activated systems can even show expansion in the long term when SAP is present [29,45,46,54,56,58,111,158,159]. Experimental results from two example studies are shown in Figs. 22 and 23. For sodium silicate-activated slag, the incorporation of SAP can restrict the drop of internal RH with little effect on the reaction products [29]. The reaction rate in the acceleration period is reduced slightly, but the elastic modulus of the matrix is not significantly influenced [29]. However, due to the existence of other driving forces like poly-condensation (see Section 3.2), the incorporation of SAP cannot fully eliminate autogenous shrinkage, especially at early age (Fig. 22).

For sodium hydroxide or sodium carbonate-activated systems, the activator acts mainly by providing high pH required for the dissolution of slag and formation of products. Without the presence of soluble silicates in the initial pore solution, the early-age extent of poly-condensation or syneresis is limited. Moreover, the high pH seems to promote the formation of hydrotalcite [160]. These may be reasons why the shrinkage of sodium hydroxide or sodium carbonate activated slag can be fully compensated by internal curing with SAP (Fig. 23).

While the effects of SAP incorporation appear promising, the internal curing liquid and dosage of SAP require caution in mix design considering that SAP can have different absorption/desorption behaviours in high concentration solutions. For cementitious materials, extra water is normally needed in the mix, to be absorbed by the SAP, while for AAMs it is possible to choose to use either extra water or extra activator [161]. If extra water is used, the activator or initial pore solution will be diluted and the reactions will be influenced (probably delayed), no matter the water is pre-absorbed by the SAP or added during mixing [47,58,162]. Using extra activator has minor influence on the reaction rate by contrast. Either way, it is important to estimate the absorption capacity of SAP before using. Some studies used tea-bag method [163–165] for this purpose, but note that SAP premixed with solid precursors may not absorb as much due to the restraint by surrounding paste as in bulk liquid, where the tea-bag is put [103]. Additionally, AAS often shows fast setting, during which the absorption of SAP in the matrix may not

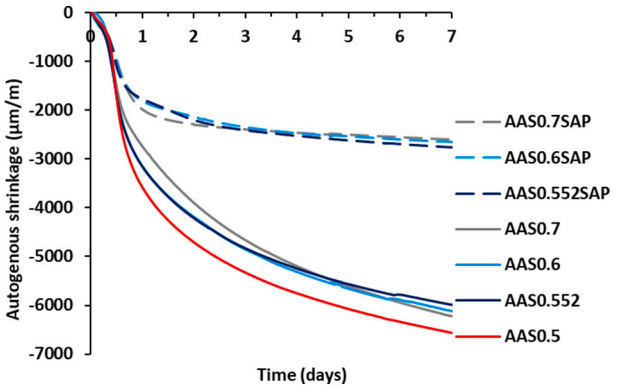

Fig. 22. Autogenous shrinkage of sodium silicate activated slag pastes with and without SAP, from [29]. The sample ID "AAS0.7SAP" denotes sodium silicate activated slag paste with l/b ratio of 0.7 and SAP; other nomenclature follows the same pattern.

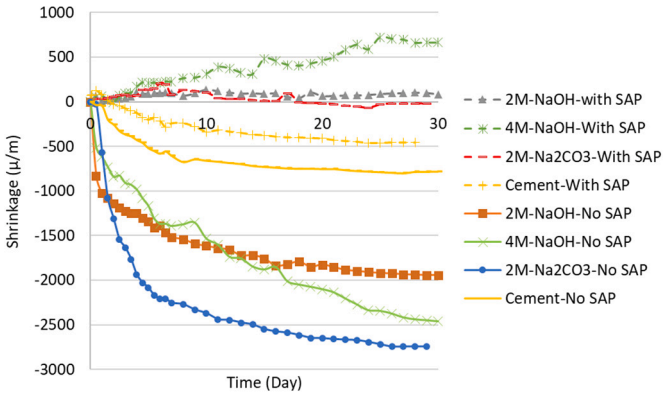

Fig. 23. Autogenous shrinkage of sodium hydroxide (NO) or sodium carbonate (NC) activated slag pastes with and without SAP, and with activator concentrations as indicated (2 M or 4 M respectively), adapted from [54].

reach its maximum [148]. To ensure sufficient internal curing liquid, one can try higher amounts of SAP than pre-designed and correspondingly extra liquid, but the strength will be further reduced [29]. The reduction in compressive strength when SAP is incorporated, regardless of dosage or introducing way, is primarily attributed to the SAP-originated voids, which act as defects and can rarely be filled by reaction products during further reaction (Fig. 24) [29].

Kumarappa et al. [46] investigated the effect of LWA in AAS mortar and observed an autogenous shrinkage reduction of up to 50 % when 30 % of the aggregates were replaced by LWA. Sakulich and Bentz [159] also obtained a greatly reduced autogenous shrinkage of AAS mortar by using LWA, regardless of the liquid used for internal curing, i.e. water or alkaline solution. However, a reduced compressive strength was also observed for the LWA-containing mixtures [159].

Beside SAP and LWA, other materials can also be used for internal curing in AAS. Lee et al. [166] used recycled concrete as internal curing aggregates for AAS concrete and found that the autogenous shrinkage can be reduced by >30 %. Along with the reduced autogenous shrinkage, the degree of hydration was decreased due to the dilution effect on the alkali activator, which was caused by the additional water supplied from the recycled aggregates. The compressive strength was only limitedly affected [166]. Zhang et al. [167] replaced part of the sand in AAS mortar with pre-soaked zeolite, and observed greatly reduced autogenous shrinkage due to the high internal RH maintained by zeolite, without any loss of compressive strength. The better effect of zeolite than LWA on the compressive strength of AAS is probably because the zeolite itself is strong, while LWA is generally weaker than normal sand [159].

Chen et al. [168] showed that perforated fly ash cenospheres can not only store and release liquid for internal curing, but also react with the activator. Their perforated cenospheres were manufactured through chemical etching, by which micron-sized holes perforating the shell of cenospheres were produced. Due to the participation of perforated cenospheres in alkali activation reactions, improvement of the compressive strength (16 %–29 %) over the control sample was achieved. Cellulose fibres can also be used as internal curing agent according to Brakat and Zhang [21]. An advantage of these fibres over SAP is that they provided reinforcement to the matrix, meaning that both the flexural and compressive strength of AAS paste can be enhanced.

6.5. Metakaolin

More than one study has identified the mitigating effect of metakaolin incorporation on the autogenous shrinkage of AAS systems [48,158,169,170]. As an aluminosilicate, metakaolin is also a commonly used precursor to synthesize AAMs [171]. When metakaolin is blended into AAS, the dosage is usually higher compared to other chemical

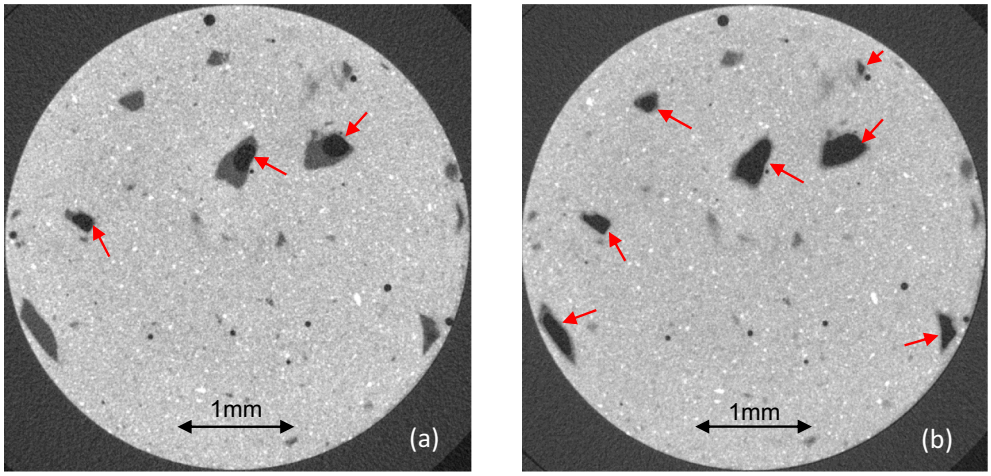

Fig. 24. A representative cross-section of AAS paste with SAP, adapted from [29]. The images were obtained by X-ray micro CT at curing ages of (a) 8 h and (b) 7 days, respectively. Several phases can be distinguished within the paste (light grey) including unreacted slag particles (white), SAP with liquid (dark grey), entrapped air (black and spherical) and the newly formed voids (black, marked by the arrows) within the SAP cavities.

admixtures such as SRA and SAP. However, the beneficial effect on mitigating autogenous shrinkage is already evident when the dosage of metakaolin reaches 10 % of the precursor, as reported by Li et al. [48]. It was found that metakaolin reduced the reaction rate of the paste and promoted the formation of highly polymerized products. Similar results were reported earlier in [172]. The pore structure of AAS paste was coarser when metakaolin was present (for alkali-activated slag with very low MgO, however, the effect on pores could be different [173]). As a result, the chemical shrinkage and drop of internal RH of the paste became lower. Similar shrinkage-mitigating mechanisms of metakaolin were reported in [64,170]. However, an issue in blended slag with metakaolin is the reduction in early-age strength together with the reduced autogenous shrinkage [64,169]. At later age, when the strength catches up, the autogenous shrinkage also develops. Hence, the mitigating effect of metakaolin on the cracking potential of AAS may not be as significant as its effect on the autogenous shrinkage [158].

6.6. *Elevated-temperature curing*

The effect of elevated-temperature curing on autogenous shrinkage of AAS has not been fully revealed yet. Ye and Radlińska [101] and Bakharev et al. [174] reported that elevated temperature curing at 60–80 °C was helpful in reducing the drying shrinkage of AAS. The reason for the observed reduction was that the viscoelastic compliance of C-A-S-H gels was reduced at elevated temperatures. This indicates that elevated temperature curing may also be effective in mitigating the autogenous shrinkage, which is critically influenced by the deformability of the gels as well [61]. As found by Uppalapati [51], the 7-day autogenous shrinkage of alkali-activated slag and fly ash mortar was mitigated by around 30 % by raising the curing temperature from 20 °C to 40 °C. In contrast to the addition of metakaolin that delayed the reaction, elevated-temperature curing accelerated the reaction; both the setting and early-age strength were promoted. Due to the accelerated reaction, the autogenous shrinkage within the first 2 days was actually increased [62]. From this point of view, it is uncertain whether elevated-temperature curing is beneficial to the cracking resistance in the early age. Moreover, this strategy may be unsuitable for cast-in-situ concrete in temperate and cold climates due to the high energy and infrastructure requirements for heated curing facilities.

6.7. *Short summary of mitigating strategies*

Based on the review in this section, it is clear that some SRA and superplasticizers that are widely adopted in PC are ineffective in AAS. Some new strategies have been developed especially for AAS, e.g. internal curing by perforated cenospheres. It is worthwhile to note that the working mechanism of any strategy in the context of AAS is never onefold. The effect on autogenous shrinkage is always coupled with other parameters, and so mitigation of autogenous shrinkage may not necessarily be associated with mitigated cracking risk. Many surfactants and internal curing agents can reduce the drop in the internal RH of AAS, but most of them delay the reaction and coarsen the microstructure, the latter of which may be unfavourable for durability. Only a few additives, such as zeolite and cellulose fibres, can mitigate the autogenous shrinkage of AAS without compromising its strength. According to the different working mechanisms of the different strategies shown above, some of these may have the potential to work synergistically if used together [148,158]. These combined approaches to autogenous shrinkage mitigation may be interesting topics for future research.

7. Remarks on testing methods

The experimental results of autogenous shrinkage of AAS systems have been reviewed in Section 2 and it was noted that the methods used by researchers were different. This should be a reason for the discrepancy in the autogenous shrinkage values of similar mixtures in different studies. Among the methods used in the literature, the corrugated tube method suggested by ASTM C1698 [175] is most widely adopted to measure length changes in AAS pastes and mortars (Fig. 25). Measurements on cubic, prismatic or cylindrical specimens were also conducted in several studies, e.g. [17,41,58,111,135,176], and volumetric methods were also used, e.g. in [65,170,177]. Some of these methods allow

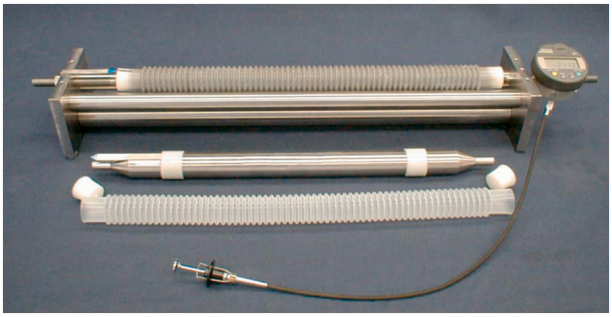

Fig. 25. Apparatus to measure the autogenous shrinkage of paste or mortar cast in a corrugated tube according to ASTM C1698, from [175].

measurement to be started immediately after casting, while the tests in other cases start only after demolding at 24 h (or earlier depending on the stiffness evolution) [30,111]. Until now, no standard has been established specially for autogenous shrinkage of AAMs; while on the other hand, it does not seem that there is any argument that the existing methods for PC-based material need significant modification to test AAS, considering their similarities in aspects of the hardening process and mechanical properties development. However, it will be useful to conduct round-robin tests to confirm this hypothesis, as is currently being done by a RILEM technical committee (TC 294-MPA).

7.1. Time-zero

Despite the possible applicability of the existing methods in measuring the autogenous shrinkage of AAS, two issues call for more attention. The first one is the starting time, or so-called "time-zero" [178,179], of the measurement. Time-zero is defined as the moment when binders form a solid skeleton to enable stress transfer. Interpreting autogenous shrinkage as from time-zero is interesting since only this part of autogenous shrinkage can cause internal tensile stress and even cracking in building materials [62]. As has been discussed in Section 3, AAS shows different rheology evolution from PC [90]. The traditional definitions of time-zero as initial setting time (e.g. by Japan Concrete Institute [114] [18]) or final setting time (e.g. by ASTM C1698 [175]) maybe be unsuitable for AAS since these moments may not correspond to the generation of internal stress [23], let alone the difficulty in accurately measuring these times.

According to the basic method of EN 196-3 [180], the Vicat setting time should be measured while the specimen is immersed in water, which is undesirable for AAMs due to the potential problem caused by leaching [181]. On the other hand, if the specimens are left in the open air in accordance with ASTM C191 [182], the surface can harden faster than the inside of the specimen due to drying effects [31]. In this case, the hardening status of the whole specimen is not homogenous and it is unclear what exactly the penetration depth of Vicat needle indicates. Therefore, it seems that a standard method to determine the setting of AAMs is needed first before discussing the use of it as the starting time of autogenous shrinkage.

For the measurement of setting time of AAS, the authors suggest application of the Vicat method, but applying sealed instead of under-water or exposed conditions to the specimen, to avoid leaching or drying of the sample (see Fig. 26). Sealing the sample, e.g. by covering it with a thin plastic wrap, during Vicat testing is believed to be practical and gives conditions close to what can be applied in practical engineering [183,184]. As demonstrated in [31], the Vicat needle can easily penetrate into the sample through the thin plastic film, and the penetration depth was barely influenced by the presence of plastic film during one penetration. The alternative method given in Annex A of EN 196–3, involving testing in a high-humidity environment, can be useful.

Compared to the use of setting time to define time-zero, Ma et al. [23] claimed that the onset of capillary pressure in alkali-activated slag and fly ash paste provides a more scientific and accurate determination of time-zero of autogenous shrinkage. The apparatus they used was a meniscus depression measuring system through which the capillary pressure could be directly measured [178]. Alternatively, Li et al. [29,63] proposed to use the starting time of the acceleration period of heat evolution as time-zero for determination of the autogenous shrinkage of alkali-activated slag and fly ash systems. They showed that both the elastic modulus and the internal tensile stress in restrained paste started to develop from that time. A disadvantage of this approach is that the determination of the boundary between dormant period and acceleration period of AAS systems can be subjective and difficult. In some systems, like sodium hydroxide-activated AAS, there can be only one major heat evolution peak with no dormant period [185], in which case, the starting time of the acceleration period would be ambiguous.

As shown in Eq. (3), the internal RH correlates with the capillary pressure. Based on that relationship, the drop of RH was suggested by Huang and Ye [186] to be used as the time-zero to indicate the building of capillary pressure. However, the starting time of the RH drop in AAMs is hard to detect due to at least two reasons. First, the pore solution of AAMs has a high (and sometimes extremely high) ionic strength, which cause a RH much lower than 100 % even without additional self-desiccation effects from the binder [29]. As explained by Raoult's law, and particularly its extension to non-ideal cases via activity coefficient formalisms, the RH in equilibrium with a solution is dependent on the molar fraction of water in the solution [187]. During alkali-activation, the ions in the pore solution are gradually consumed by reaction and incorporation into the solid binder phase, and so their concentrations decrease, making it possible that the overall RH of the paste may even increase as reaction proceeds [58,188]. Second, the temperature of a RH measurement chamber is difficult to accurately control when the sample is undergoing an exothermic reaction process. Due to the reaction heat, the specimen can be slightly hotter than the sensor, and water vapour can condense on the sensor surface [186]. In such cases, a RH value close to 100 % will be measured even when the actual RH of the specimen is not so high. The condensation problem can be more severe for mixtures that show bleeding on their surface [62].

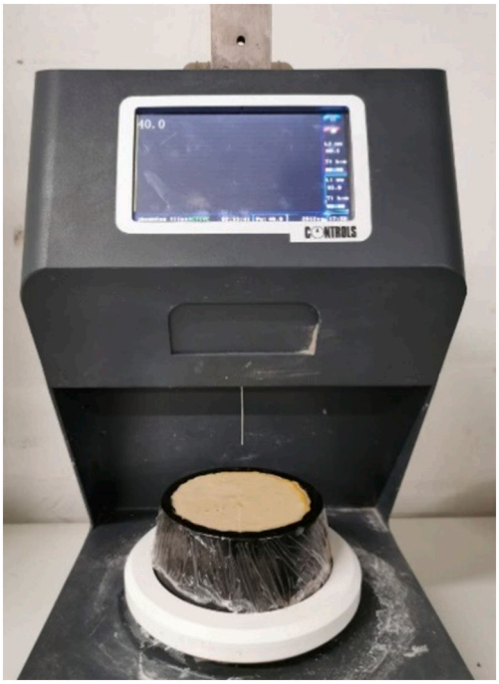

Fig. 26. Vicat apparatus to measure the setting time of AAS paste, which was sealed by plastic film, adapted from [73].

The time-zero for autogenous shrinkage of AAS can also be determined according to the stiffness evolution of the material. Ultrasonic P-wave velocity testing, and the Elasticity Modulus Monitoring through Ambient Response Method (EMM-ARM), have been found to be feasible for this purpose [63,189], and the time-zero can be identified as the knee-point of the curves of P-wave velocity or the elastic modulus. Of course, the knee-point times obtained through these two methods may not be identical due to the differences between the dynamic and quasi-static elastic moduli of a material, an issue that has been well known from studies on PC [190].

Another way to determine the time-zero is by using a ring test or TSTM to monitor the stress evolution in restrained AAS paste, mortar or concrete [158]. The moment when the stress starts to surge should be the time-zero. However, a disadvantage of these approaches is that the experiments are complex and time consuming.

7.2. Duration of measurement

Another issue of concern when measuring the autogenous shrinkage of AAS is the test duration. For PC-based systems, the autogenous shrinkage is usually measured for 28 days, or even only 7 days [191–193]. This is reasonable because the hydration and self-desiccation of PC develop rapidly at early age, and the autogenous shrinkage increases only marginally after the formation of a stable skeleton. For AAS, by contrast, the reaction degree can be lower than that of PC in the first days [75]. Moreover, the pronounced viscosity of the reaction products enables a large extent of creep to take place, which contributes to the development of autogenous shrinkage in the long run [194]. Hence, a measurement that lasts for 7 days might be insufficient when studying the autogenous shrinkage of AAS.

Many more experimental data on the influences of various parameters are needed to establish standards or codes for the measurement of autogenous shrinkage of AAMs. Using unified definitions of starting and ending times of the measurement is a critical step toward that, to make the results from different researchers and laboratories comparable.

8. Conclusions

In this paper, we provide a systematic literature review on the autogenous shrinkage of AAS, currently the most widely used AAM system. Several issues including the magnitude, mechanism and modelling of autogenous shrinkage, cracking tendency resulting from restrained autogenous shrinkage, and shrinkage-mitigating strategies are reviewed. Remarks are also given on testing methods for autogenous shrinkage of AAS. Suggestions for future research in these fields are provided. Based on the review, the following conclusions can be drawn:

- The autogenous shrinkage of AAS systems is generally higher than PC-based counterparts with similar strength. A higher dosage of alkali, a lower water/binder ratio, or silicate activator modulus closer to 1.0 tends to result in a higher autogenous shrinkage of AAS.
- Capillary pressure generated during the self-desiccation process is the main driving force of the autogenous shrinkage of hardened AAS. The large surface tension of the pore solution, dense pore structure, and high saturation degree all contribute to the large capillary pressure in AAS. The deformability of AAS is evident due to the pronounced viscoelasticity of C-A-S-H gels.
- Besides self-desiccation, other mechanisms also play roles especially in the hardening stage, such as the polycondensation of gel particles and the decrease of steric-hydration forces due to the consumption of ions from the pore solution. However, these hypotheses are not yet fully supported by experimental evidence.
- Compared with the curing age, the DoR seems to correspond better with the development of autogenous shrinkage of AAS. Existing models for PC do not give satisfactory estimations unless the pronounced viscoelasticity of AAS is considered.
- The tendency of AAS systems to suffer from thorough cracking is not necessarily high due to stress relaxation effects, but local creep can cause new stress concentration in other zones and aggravate the development of microcracking.
- Some admixtures that are widely adopted in PC lose their function in AAS. Internal curing is effective in mitigating the autogenous shrinkage of AAS, but may also delay the reaction and/or coarsen the microstructure. Only a few strategies can mitigate the autogenous shrinkage of AAS without compromising its strength.
- Existing experimental methods, such as the corrugated tube method, seem applicable for AAS systems, but the definition of time-zero and the duration of measurement need to be carefully considered.

In general, the research attention that has been paid to volume stability issues in AAS is not yet sufficient. A clearer understanding of the autogenous shrinkage is important not only because it can potentially cause cracking, but also because it plays a considerable role in other deformation processes such as drying shrinkage, thermal deformation and creep, which can be more problematic in some scenarios. Strategies that can mitigate the shrinkage of AAS without harming its microstructure are desired.

CRediT authorship contribution statement

Zhenming Li: Conceptualization, Investigation, Writing – original draft, Writing – review & editing. **Yun Chen:** Investigation, Data curation. **John L. Provis:** Writing – review & editing. **Özlem Cizer:** Writing – review & editing. **Guang Ye:** Supervision, Writing – review & editing.

Declaration of competing interest

The authors declare that they have no known competing financial interests or personal relationships that could have appeared to influence the work reported in this paper.

Data availability

Data will be made available on request.

Acknowledgement

This work was partially supported by Horizon Europe guarantee funding (grant number EP/X022587/1). The first author (ZL) would like to thank Prof. Klaas van Breugel for the insightful discussions with him. The second author (YC) would like to acknowledge the financial support from China Scholarship Council (Grant No. 201906150022). The contributions of JLP were supported by the Engineering and Physical Sciences Research Council (UK) under grant number EP/S019650/1.

Appendix A

Table A1

Autogenous shrinkage (AS) of AAS measured in literature. The table is categorized based on the presence of aggregates, and in each category the table is sorted based by the type of alkaline activator (AA) and Na_2O content. The content of Na_2O is defined relative to the weight of slag. M_s, w/b, and T represent modulus (molar ratio of SiO_2/Na_2O) of the activator, water/binder ratio and curing temperature, respectively. NS, NH, Nc and N$ stand for sodium silicate, sodium hydroxide, sodium carbonate and sodium sulfate solution, respectively. NS powder indicates that solid NS was used as the activator. The sign "–" is put when the information is inapplicable, unmentioned or unidentifiable.

System	AA	Na_2O	M_s	w/b	T (°C)	Shape of specimen	Magnitude of AS (μm/m unless noted)			References
							1 d	7 d	28 d	
Paste	NS	1 %	0.6	0.26	25	Prism	–	200	300	Allahverdi et al. [195]
Paste	NS	2 %	0.6	0.26	25	Prism	–	600	800	Allahverdi et al. [195]

(continued on next page)

Table A1 (*continued*)

System	AA	Na_2O	M_s	w/b	T (°C)	Shape of specimen	Magnitude of AS (μm/m unless noted)			References
							1 d	7 d	28 d	
Paste	NS	4 %	1.2	0.35	20	Condom	0.022 ml/g	0.033 ml/g	–	He et al. [70]
Paste	NS	4 %	1.96	0.35	25	Prisms	0	5600	9500	Kalina et al. [65]
Paste	NS	4 %	0.5	0.4	20	Corrugated tube	1300	3000	–	Chen et al. [22]
Paste	NS	4 %	1.0	0.4	20	Corrugated tube	200	3700	–	Chen et al. [22]
Paste	NS	4 %	1.5	0.4	20	Corrugated tube	200	4300	–	Chen et al. [22]
Paste	NS	4 %	2.0	0.4	20	Corrugated tube	300	4600	–	Chen et al. [22]
Paste	NS	4 %	1.2	0.4	20	Corrugated tube	2300	4900	–	Brakat et al. [21]
Paste	NS	4 %	1.5	0.4	20	Corrugated tube	4800	7800		Ma et al. [23]
Paste	NS	4 %	1.2	0.4	20	Corrugated tube	1900	–	–	Cao et al. [196]
Paste	NS	4 %	1.2	0.4	20	Prisms	–	3000	4900	Cao et al. [196]
Paste	NS	4 %	0.8	0.5	20	Corrugated tube	1600	4200	–	Jiang et al. [45]
Paste	NS	4 %	1	0.5	20	Corrugated tube	800	4800	–	Jiang et al. [45]
Paste	NS	4 %	1.4	0.5	20	Corrugated tube	300	4600	–	Jiang et al. [45]
Paste	NS	4.7 %	1.5	0.34	20	Corrugated tube	3700	6700	–	Li et al. [30]
Paste	NS	4.7 %	1.5	0.38	20	Corrugated tube	3500	6500	–	Li et al. [30]
Paste	NS	4.7 %	1.5	0.38	20	Corrugated tube	3500	6500	–	Li et al. [29]
Paste	NS	5 %	0.5	0.43	20	Corrugated tube	2000	3900	–	Li et al. [31]
Paste	NS	5 %	1	0.43	20	Corrugated tube	200	4200	–	Li et al. [31]
Paste	NS	5 %	1.5	0.43	20	Corrugated tube	3200	6400	–	Li et al. [31]
Paste	NS	5.2 %	1.5	0.43	20	Corrugated tube	3100	5900	–	Li et al. [29]
Paste	NS	5.7 %	1.5	0.46	20	Corrugated tube	3100	6000	–	Li et al. [29]
Paste	NS	6 %	0.5	0.4	20	Corrugated tube	2200	4300	–	Chen et al. [22]
Paste	NS	6 %	1.0	0.4	20	Corrugated tube	5500	8000	–	Chen et al. [22]
Paste	NS	6 %	1.5	0.4	20	Corrugated tube	3500	6000	–	Chen et al. [22]
Paste	NS	6 %	2.0	0.4	20	Corrugated tube	2200	4300	–	Chen et al. [22]
Paste	NS	6 %	1	0.4	20	Prism	800	2500	3900	Abate et al. [55]
Paste	NS	6 %	1	0.45	20	Prism	400	2200	3800	Abate et al. [55]
Paste	NS	6 %	1	0.5	20	Prism	500	1800	3200	Abate et al. [55]
Paste	NS	6.2 %	1.2	0.45	20	Corrugated tube	700	2800	5000	Yu et al. [57]
Paste	NS	6.2 %	1.2	0.45	20	Corrugated tube	700	2100	3600	Yu et al. [52]
Paste	NS	6.7 %	1.5	0.54	20	Corrugated tube	2800	6200	–	Li et al. [29]
Paste	NS	8 %	0.5	0.4	20	Corrugated tube	3000	4900	–	Chen et al. [22]
Paste	NS	8 %	1.0	0.4	20	Corrugated tube	5500	8200	–	Chen et al. [22]
Paste	NS	8 %	1.5	0.4	20	Corrugated tube	4000	6500	–	Chen et al. [22]
Paste	NS	8 %	2.0	0.4	20	Corrugated tube	2000	4300	–	Chen et al. [22]
Paste	NS	9.3 %	0.76	0.42	20	Corrugated tube	5000	6900	–	Li et al. [48]
Paste	NS	10 %	1	0.4	20	Prism	1600	3400	5500	Abate et al. [55]
Paste	NS	10 %	1	0.45	20	Prism	1500	3300	5200	Abate et al. [55]
Paste	NS	10 %	1	0.5	20	Prism	600	3000	5200	Abate et al. [55]
Paste	NS	14 %	1	0.4	20	Prism	1200	2600	4800	Abate et al. [55]
Paste	NS	14 %	1	0.45	20	Prism	1000	2500	4200	Abate et al. [55]
Paste	NS	14 %	1	0.5	20	Prism	1400	3200	5600	Abate et al. [55]
Paste	NS powder	1.8 %	1	0.4	20	Prism	–	2500	4000	Abate et al. [55]
Paste	NS powder	1.8 %	1	0.45	20	Prism	–	2200	3600	Abate et al. [55]
Paste	NS powder	1.8 %	1	0.5	20	Prism	–	1800	3200	Abate et al. [55]
Paste	NS powder	3.2 %	1	0.4	20	Prism	–	3400	5800	Abate et al. [55]
Paste	NS powder	3.2 %	1	0.45	20	Prism	–	3300	5600	Abate et al. [55]
Paste	NS powder	3.2 %	1	0.5	20	Prism	–	3000	5500	Abate et al. [55]
Paste	NS powder	4 %	1.54	0.45	20	Prisms	–	1100	–	Yin et al. [197]
Paste	NS powder	4.8 %	1	0.4	20	Prism	–	3000	4800	Abate et al. [55]
Paste	NS powder	4.8 %	1	0.45	20	Prism	–	2600	4500	Abate et al. [55]
Paste	NS powder	4.8 %	1	0.5	20	Prism	–	3200	5500	Abate et al. [55]
Paste	NS powder	5 %	1	0.35	20	Corrugated tube	1000	3200	5400	Chen et al. [102]
Paste	NH	2 %	–	0.35	23	Corrugated tube	800	1500	1800	Vafaei et al. [54]
Paste	NH	4 %	–	0.4	20	Corrugated tube	1000	–	–	Cao et al. [196]
Paste	NH	4 %	–	0.4	20	Prisms	–	1000	2200	Cao et al. [196]
Paste	NH	4.7 %	–	0.38	23	Corrugated tube	500	1400	2500	Vafaei et al. [54]
Paste	Nc	4 %	–	0.4	20	Condom	0.003 ml/g	0.013 ml/g	–	Zheng et al. [59]
Paste	Nc	4.7 %	–	0.38	23	Corrugated tube	600	2200	2700	Vafaei et al. [54]
Paste	NŚ	4 %	–	0.4	20	Condom	0.004 ml/g	0.015 ml/g	–	Zheng et al. [59]

System	Paste mass%	AA	Na_2O	M_s	w/b	T (°C)	Shape of specimen	Magnitude of AS (μm/m unless noted)			References
								1 d	7 d	28 d	
Mortar	43 %	NS	2.5 %	1.7	0.48	24	Prism	100	500	1200	Neto et al. [17]
Mortar	43 %	NS	3.5 %	1.7	0.48	24	Prism	0	1100	1600	Neto et al. [17]
Mortar	43 %	NS	3.6 %	1.2	0.47	23	Corrugated tube	–	800	1300	Cartwright et al. [40]
Mortar	55 %	NS	4 %	1.2	0.4	23	Prism	20	170	350	Song et al. [111]
Mortar	43 %	NS	4 %	0.4	0.47	23	Corrugated tube	–	400	1000	Cartwright et al. [40]
Mortar	53 %	NS	4 %	1.5	0.4	21	Corrugated tube	–	2000	2500	Kumarappa et al. [46]
Mortar	43 %	NS	4 %	1.5	0.4	20	Corrugated tube	600	1050	–	You et al. [198]

(*continued on next page*)

Table A1 (*continued*)

System	Paste mass%	AA	Na_2O	M_s	w/b	T (°C)	Shape of specimen	Magnitude of AS (μm/m unless noted)			References
								1 d	7 d	28 d	
Mortar	43 %	NS	4.5 %	1.7	0.48	24	Prism	900	2100	2500	Neto et al. [17]
Mortar	35 %	NS	5 %	2	0.5	20	Prism	750	1150	–	Yang et al. [148]
Mortar	33 %	NS	5 %	1.2	0.4	20	Prism	110	1000	–	Zhu et al. [42]
Mortar	35 %	NS	5 %	1.8	0.5	20	Prism	–	1300	1850	Liu et al. [134]
Mortar	53 %	NS	5 %	1.5	0.4	21	Corrugated tube	–	2200	3200	Kumarappa et al. [46]
Mortar	53 %	NS	5 %	0.75	0.4	21	Corrugated tube	–	1500	2500	Kumarappa et al. [46]
Mortar	53 %	NS	5 %	1.75	0.4	21	Corrugated tube	–	2500	3800	Kumarappa et al. [46]
Mortar	39 %	NS	5.6 %	0.56	0.4	20	Corrugated tube	450	900	–	Oh et al. [199]
Mortar	53 %	NS	6 %	1.5	0.4	21	Corrugated tube	–	3000	4200	Kumarappa et al. [46]
Mortar	33 %	NS	6 %	1	0.45	20	Condom	4.5 %	5.6 %	–	Fu et al. [169]
Mortar	36 %	NS	7.5 %	1.28	0.53	20	Corrugated tube	800	1650	–	Uppalapati et al. [200]
Mortar	60 %	NS	8 %	1.8	0.4	23	Corrugated tube	200	900	2000	Chen et al. [168]
Mortar	37 %	NS	–	–	–	25	Corrugated tube	–	2400	3400	Sakulich et al. [159]
Mortar	42 %	NH	3 %	–	0.47	20	Corrugated tube	–	0	300	Cartwright et al. [40]
Mortar	33 %	NH	4 %	–	0.4	20	Prism	–	300	700	Zheng et al. [60]
Mortar	–	NH	4 %	–	0.5	23	Prism	10	90	200	Rifai et al. [126]
Mortar	43 %	NH	5 %	–	0.48	24	Prism	50	250	600	Cincotto et al. [53]
Mortar	43 %	NH	6 %	–	0.45	20	Corrugated tube	–	200	800	Cartwright et al. [40]
Mortar	35 %	NH	9.1 %	–	0.53	20	Corrugated tube	450	450	–	Uppalapati et al. [200]
Mortar	55 %	NH	10 %	–	0.37	23	Prism	300	800	1700	Wang et al. [56]
Mortar	44 %	NH	–	–	–	20	Corrugated tube	40	325	–	Zhang et al. [161]
Mortar	–	NH	–	–	0.5	25	Prism	10	80	200	Rifai et al. [201]
Mortar	38 %	Nc	4 %	–	0.4	23	Prism	0	70	190	Song et al. [111]
Mortar	38 %	Nc	6.4 %	–	0.4	20	Corrugated tube	25	125	–	Oh et al. [199]
Mortar	35 %	Nc	–	–	–	25	Corrugated tube	–	700	1300	Sakulich et al. [159]
Concrete	28 %	NS	4.2 %	0.9	0.41	20	Prism	–	90	200	Ma et al. [50]
Concrete	25 %	NS	4.8 %	1.5	0.38	20	Prism	100	400	–	Li et al. [124]
Concrete	25 %	NS	5 %	1.2	0.45	20	Prism	150	350	470	Zhu et al. [96]
Concrete	26 %	NS	5 %	1.2	0.52	20	Prism	50	340	500	Zhu et al. [96]
Concrete	25 %	NS	8 %	1	0.5	20	Prism	50	680	–	Huang et al. [44]
Concrete	21 %	NS	10 %	1	0.45	20	Cylinder	50	370	900	Humad et al. [135]

References

[1] C. Shi, B. Qu, J.L. Provis, Recent progress in low-carbon binders, Cem. Concr. Res. 122 (2019) 227–250, https://doi.org/10.1016/j.cemconres.2019.05.009.

[2] S.A. Bernal, J.L. Provis, A. Fernández-jiménez, P.V. Krivenko, E. Kavalerova, M. Palacios, C. Shi, Alkali activated materials, 2014, https://doi.org/10.1007/978-94-007-7672-2.

[3] P. Awoyera, A. Adesina, A critical review on application of alkali activated slag as a sustainable composite binder, Case Stud. Constr. Mater. 11 (2019), e00268.

[4] G. Habert, S.A. Miller, V.M. John, J.L. Provis, A. Favier, A. Horvath, K. L. Scrivener, Environmental impacts and decarbonization strategies in the cement and concrete industries, Nat. Rev. Earth Environ. 1 (2020) 559–573.

[5] J.L. Provis, J.S.J. Van Deventer, Alkali activated materials, 2014, https://doi.org/10.1007/978-94-007-7672-2.

[6] K. Arbi, M. Nedeljković, Y. Zuo, G. Ye, A review on the durability of alkali-activated fly ash/slag systems: advances, issues, and perspectives, Ind. Eng. Chem. Res. 55 (2016) 5439–5453, https://doi.org/10.1021/acs.iecr.6b00559.

[7] B. Zhang, H. Zhu, P. Feng, P. Zhang, A review on shrinkage-reducing methods and mechanisms of alkali-activated/geopolymer systems: effects of chemical additives, J. Build. Eng. (2022), 104056, https://doi.org/10.1016/j.jobe.2022.104056.

[8] M.S. Sule, Effect of Reinforcement on Early-age Cracking in High Strength Concrete, Delft University of Technology, 2003.

[9] P. Lura, Autogenous Deformation And Internal Curing of Concrete, Delft University of Technology, 2003.

[10] B. Zhang, H. Zhu, Y. Cheng, G.F. Huseien, K.W. Shah, Shrinkage mechanisms and shrinkage-mitigating strategies of alkali-activated slag composites: a critical review, Constr. Build. Mater. 318 (2022), 125993, https://doi.org/10.1016/j.conbuildmat.2021.125993.

[11] M. Mastali, P. Kinnunen, A. Dalvand, R. Mohammadi Firouz, M. Illikainen, Drying shrinkage in alkali-activated binders – a critical review, Constr. Build. Mater. 190 (2018) 533–550, https://doi.org/10.1016/j.conbuildmat.2018.09.125.

[12] S. Wang, X. Pu, K.L. Scrivener, P.L. Pratt, Alkali-activated slag cement and concrete: a review of properties and problems, Adv. Cem. Res. 7 (1995) 93–102, https://doi.org/10.1680/adcr.1995.7.27.93.

[13] Z. Li, J. Liu, G. Ye, Drying shrinkage of alkali-activated slag and fly ash concrete; a comparative study with ordinary Portland cement concrete, Heron 64 (2019) 149.

[14] H. Wu, Improving freeze-thaw resistance of alkali-activated slag by admixtures, 2023.

[15] S.A. Bernal, R.M. de Gutierrez, J.L. Provis, V. Rose, Effect of silicate modulus and metakaolin incorporation on the carbonation of alkali silicate-activated slags, Cem. Concr. Res. 40 (2010) 898–907, https://doi.org/10.1016/j.cemconres.2010.02.003.

[16] O.M. Jensen, P.F. Hansen, Autogenous deformation and RH-change in perspective, Cem. Concr. Res. 31 (2001) 1859–1865, https://doi.org/10.1016/S0008-8846(01)00501-4.

[17] A.A. Melo Neto, M.A. Cincotto, W. Repette, Drying and autogenous shrinkage of pastes and mortars with activated slag cement, Cem. Concr. Res. 38 (2008) 565–574, https://doi.org/10.1016/j.cemconres.2007.11.002.

[18] Y. Gu, Y. Fang, Shrinkage, cracking, shrinkage-reducing and toughening of alkali-activated slag cement - a short review, J. Chin. Ceram. Soc. 40 (2012) 76–84.

[19] Y. Zuo, M. Nedeljković, G. Ye, Coupled thermodynamic modelling and experimental study of sodium hydroxide activated slag, Constr. Build. Mater. 188 (2018) 262–279, https://doi.org/10.1016/J.CONBUILDMAT.2018.08.087.

[20] B. Sun, G. Ye, G. de Schutter, A review: reaction mechanism and strength of slag and fly ash-based alkali-activated materials, Constr. Build. Mater. 326 (2022), 126843, https://doi.org/10.1016/j.conbuildmat.2022.126843.

[21] A. Brakat, Y. Zhang, Shrinkage mitigation of alkali-activated slag with natural cellulose fibres, Adv. Cem. Res. 31 (2019) 47–57, https://doi.org/10.1680/jadcr.17.00147.

[22] W. Chen, B. Li, J. Wang, N. Thom, Effects of alkali dosage and silicate modulus on autogenous shrinkage of alkali-activated slag cement paste, Cem. Concr. Res. 141 (2021), https://doi.org/10.1016/j.cemconres.2020.106322.

[23] Y. Ma, X. Yang, J. Hu, Z. Zhang, H. Wang, Accurate determination of the "time-zero" of autogenous shrinkage in alkali-activated fly ash/slag system, Compos. Part B 177 (2019), https://doi.org/10.1016/j.compositesb.2019.107367.

[24] M. Nedeljković, Z. Li, G. Ye, Setting, strength, and autogenous shrinkage of alkali-activated fly ash and slag pastes: effect of slag content, Materials 11 (2018) 2121, https://doi.org/10.3390/ma11112121.

[25] Y. Zuo, Experimental Study And Numerical Simulation of the Reaction Process And Microstructure Formation of Alkali-activated Materials, Delft University of Technology, 2019.

[26] H. Taghvayi, K. Behfarnia, M. Khalili, The effect of alkali concentration and sodium silicate modulus on the properties of alkali-activated slag concrete, J. Adv. Concr. Technol. 16 (2018) 293–305.

[27] X. Ouyang, Y. Ma, Z. Liu, J. Liang, G. Ye, Effect of the sodium silicate modulus and slag content on fresh and hardened properties of alkali-activated fly ash/slag, Minerals. 10 (2019) 15.

[28] M.H. Zhang, C.T. Tam, M.P. Leow, Effect of water-to-cementitious materials ratio and silica fume on the autogenous shrinkage of concrete, Cem. Concr. Res. 33 (2003) 1687–1694, https://doi.org/10.1016/S0008-8846(03)00149-2.

[29] Z. Li, M. Wyrzykowski, H. Dong, J. Granja, M. Azenha, P. Lura, G. Ye, Internal curing by superabsorbent polymers in alkali-activated slag, Cem. Concr. Res. 135 (2020), 106123, https://doi.org/10.1016/j.cemconres.2020.106123.

[30] Z. Li, T. Lu, Y. Chen, B. Wu, G. Ye, Prediction of the autogenous shrinkage and microcracking of alkali-activated slag and fly ash concrete, Cem. Concr. Compos. 117 (2021), https://doi.org/10.1016/j.cemconcomp.2020.103913.

[31] Z. Li, I.A.F. Beltran, Y. Chen, B. Šavija, G. Ye, Early-age properties of alkali-activated slag and glass wool paste, Constr. Build. Mater. 291 (2021), 123326, https://doi.org/10.1016/j.conbuildmat.2021.123326.

[32] A. Mehta, R. Siddique, An overview of geopolymers derived from industrial by-products, Constr. Build. Mater. 127 (2016) 183–198, https://doi.org/10.1016/j.conbuildmat.2016.09.136.

[33] S.A. Bernal, R. San Nicolas, R.J. Myers, R.M. de Gutiérrez, F. Puertas, J.S.J. van Deventer, J.L. Provis, MgO content of slag controls phase evolution and structural changes induced by accelerated carbonation in alkali-activated binders, Cem. Concr. Res. 57 (2014) 33–43.

[34] S. Blotevogel, A. Ehrenberg, L. Steger, L. Doussang, J. Kaknics, C. Patapy, M. Cyr, Ability of the R3 test to evaluate differences in early age reactivity of 16 industrial ground granulated blast furnace slags (GGBS), Cem. Concr. Res. 130 (2020), 105998.

[35] T. Luukkonen, Z. Abdollahnejad, J. Yliniemi, P. Kinnunen, M. Illikainen, One-part alkali-activated materials: a review, Cem. Concr. Res. 103 (2018) 21–34, https://doi.org/10.1016/j.cemconres.2017.10.001.

[36] P. Lura, M. Wyrzykowski, Influence of aggregate restraint on volume changes: experiments and modelling, in: Concreep, 2015, pp. 17–23, https://doi.org/10.1061/9780784479346.

[37] E. ichi Tazawa, S. Miyazawa, T. Kasai, Chemical shrinkage and autogenous shrinkage of hydrating cement paste, Cem. Concr. Res. 25 (1995) 288–292, https://doi.org/10.1016/0008-8846(95)00011-9.

[38] E. ichi Tazawa, S. Miyazawa, Influence of cement and admixture on autogenous shrinkage of cement paste, Cem. Concr. Res. 25 (1995) 281–287, https://doi.org/10.1016/0008-8846(95)00010-0.

[39] V. Baroghel-Bouny, P. Mounanga, A. Khelidj, A. Loukili, N. Rafaï, Autogenous deformations of cement pastes: part I. Temperature effects at early age and micro–macro correlations, Cem. Concr. Res. 36 (2006) 123–136, https://doi.org/10.1016/j.cemconres.2004.10.020.

[40] C. Cartwright, F. Rajabipour, A. Radli, Shrinkage characteristics of alkali-activated slag cements, J. Mater. Civ. Eng. 27 (2014) 1–9, https://doi.org/10.1061/(ASCE)MT.1943-5533.0001058.

[41] L. Xie, K. Liu, Properties and microstructure of Na2CO3-activated binders modified with Ca(OH)2 and Mg(OH)2 15 (2022) 1687.

[42] X. Zhu, X. Kang, J. Deng, K. Yang, L. Yu, C. Yang, A comparative study on shrinkage characteristics of graphene oxide (GO) and graphene nanoplatelets (GNPs) modified alkali-activated slag cement composites, Mater. Struct. Constr. 54 (2021) 1–15, https://doi.org/10.1617/s11527-021-01695-w.

[43] N.K. Lee, J.G. Jang, H.K. Lee, Shrinkage characteristics of alkali-activated fly ash/slag paste and mortar at early ages, Cem. Concr. Compos. 53 (2014) 239–248, https://doi.org/10.1016/j.cemconcomp.2014.07.007.

[44] J. Huang, J. Yan, K. Liu, B. Wei, C. Zou, Influence of cooking oil on the mitigation of autogenous shrinkage of alkali-activated slag concrete, Materials 13 (2020) 1–19, https://doi.org/10.3390/ma13214907.

[45] D. Jiang, X. Li, Y. Lv, C. Li, W. Jiang, Z. Liu, J. Xu, Y. Zhou, J. Dan, Autogenous shrinkage and hydration property of alkali activated slag pastes containing superabsorbent polymer, Cem. Concr. Res. 149 (2021), 106581, https://doi.org/10.1016/j.cemconres.2021.106581.

[46] B.D. Kumarappa, S. Peethamparan, M. Ngami, Autogenous shrinkage of alkali activated slag mortars: basic mechanisms and mitigation methods, Cem. Concr. Res. 109 (2018) 1–9, https://doi.org/10.1016/j.cemconres.2018.04.004.

[47] A. Rodrigue, J. Duchesne, B. Fournier, B. Bissonnette, Influence of added water and fly ash content on the characteristics, properties and early-age cracking sensitivity of alkali-activated slag/fly ash concrete cured at ambient temperature, Constr. Build. Mater. 171 (2018) 929–941, https://doi.org/10.1016/j.conbuildmat.2018.03.176.

[48] Z. Li, M. Nedeljković, B. Chen, G. Ye, Mitigating the autogenous shrinkage of alkali-activated slag by metakaolin, Cem. Concr. Res. 122 (2019) 30–41, https://doi.org/10.1016/j.cemconres.2019.04.016.

[49] Z. Li, S. Zhang, X. Liang, J. Granja, M. Azenha, G. Ye, Internal curing of alkali-activated slag-fly ash paste with superabsorbent polymers, Constr. Build. Mater. 263 (2020), 120985, https://doi.org/10.1016/j.conbuildmat.2020.120985.

[50] J. Ma, F. Dehn, Shrinkage and creep behavior of an alkali-activated slag concrete, Struct. Concr. 18 (2017) 801–810, https://doi.org/10.1002/suco.201600147.

[51] S. Uppalapati, L. Vandewalle, Ö. Cizer, Autogenous shrinkage of slag-fly ash blends activated with hybrid sodium silicate and sodium sulfate at different curing temperatures, Constr. Build. Mater. 265 (2020), 121276, https://doi.org/10.1016/j.conbuildmat.2020.121276.

[52] Z.Y. Qu, Q. Yu, Y.D. Ji, F. Gauvin, I.K. Voets, Mitigating shrinkage of alkali activated slag with biofilm, Cem. Concr. Res. 138 (2020), 106234, https://doi.org/10.1016/j.cemconres.2020.106234.

[53] M.A. Cincotto, A.A. Melo Neto, W. Repette, Effect of different activators type and dosages and relation to autogenous shrinkage of activated blast furnace slag cement, in: 11th Int. Congr. Chem. Cem, 2003, pp. 1878–1888.

[54] B. Vafaei, K. Farzanian, A. Ghahremaninezhad, The influence of superabsorbent polymer on the properties of alkali-activated slag pastes, Constr. Build. Mater. 236 (2020), 117525, https://doi.org/10.1016/j.conbuildmat.2019.117525.

[55] S.Y. Abate, S. Park, H.K. Kim, Parametric modeling of autogenous shrinkage of sodium silicate-activated slag, Constr. Build. Mater. 262 (2020), 120747, https://doi.org/10.1016/j.conbuildmat.2020.120747.

[56] P. Wang, H. Chen, P. Chen, J. Pan, Y. Xu, H. Wang, W. Shen, K. Cao, Effect of internal curing by super absorbent polymer on the autogenous shrinkage of alkali-activated slag mortars, Materials 13 (2020) 1–13, https://doi.org/10.3390/ma13194318.

[57] Z.Y. Qu, F. Gauvin, F.Z. Wang, G. Liu, H.J.H. Brouwers, Effect of hydrophobicity on autogenous shrinkage and carbonation of alkali activated slag, Constr. Build. Mater. 264 (2020), https://doi.org/10.1016/j.conbuildmat.2020.120665.

[58] W. Tu, Y. Zhu, G. Fang, X. Wang, M. Zhang, Internal curing of alkali-activated fly ash-slag pastes using superabsorbent polymer, Cem. Concr. Res. 116 (2019) 179–190, https://doi.org/10.1016/j.cemconres.2018.11.018.

[59] W. Zheng, J. He, Y. Tong, J. He, X. Song, G. Sang, Investigation of effects of reactive MgO on autogenous and drying shrinkage of near-neutral salt activated slag cement, Ceram. Int. 48 (2022) 5518–5526, https://doi.org/10.1016/j.ceramint.2021.11.096.

[60] D. Zheng, T. Ji, G. Wang, Effect of CaO on the autogenous shrinkage of alkali-activated slag mortar, Adv. Mater. Sci. Eng. 2021 (2021), https://doi.org/10.1155/2021/9918834.

[61] H. Ye, A. Radlińska, Shrinkage mechanisms of alkali-activated slag, Cem. Concr. Res. 88 (2016) 126–135, https://doi.org/10.1016/j.cemconres.2016.07.001.

[62] S. Uppalapati, Early-age Structural Development And Autogenous Shrinkage of Alkali-activated Slag/Fly-ash Cements, KU Leuven, 2021.

[63] Z. Li, T. Lu, X. Liang, H. Dong, G. Ye, Mechanisms of autogenous shrinkage of alkali-activated slag and fly ash pastes, Cem. Concr. Res. 135 (2020), 106107, https://doi.org/10.1016/j.cemconres.2020.106107.

[64] Z. Li, X. Liang, Y. Chen, G. Ye, Effect of metakaolin on the autogenous shrinkage of alkali-activated slag-fly ash paste, Constr. Build. Mater. 278 (2021), 122397, https://doi.org/10.1016/j.conbuildmat.2021.122397.

[65] L. Kalina, V. Bílek, E. Bartoníčková, M. Kalina, J. Hajzler, R. Novotný, Doubts over capillary pressure theory in context with drying and autogenous shrinkage of alkali-activated materials, Constr. Build. Mater. 248 (2020), https://doi.org/10.1016/j.conbuildmat.2020.118620.

[66] G. Fang, H. Bahrami, M. Zhang, Mechanisms of autogenous shrinkage of alkali-activated fly ash-slag pastes cured at ambient temperature within 24 h, Constr. Build. Mater. 171 (2018) 377–387, https://doi.org/10.1016/j.conbuildmat.2018.03.155.

[67] Z. Li, M. Nedeljkovic, Y. Zuo, G. Ye, Autogenous shrinkage of alkali-activated slag-fly ash pastes, in: 5th Int. Slag Valoris. Symp, 2017, pp. 369–372. Leuven.

[68] J.J. Thomas, A.J. Allen, H.M. Jennings, Density and water content of nanoscale solid C-S-H formed in alkali-activated slag (AAS) paste and implications for chemical shrinkage, Cem. Concr. Res. 42 (2012) 377–383, https://doi.org/10.1016/j.cemconres.2011.11.003.

[69] S. Hanjitsuwan, B. Injorhor, T. Phoo-ngernkham, N. Damrongwiriyanupap, L. Y. Li, P. Sukontasukkul, P. Chindaprasirt, Drying shrinkage, strength and microstructure of alkali-activated high-calcium fly ash using FGD-gypsum and dolomite as expansive additive, Cem. Concr. Compos. 114 (2020), 103760, https://doi.org/10.1016/j.cemconcomp.2020.103760.

[70] J. He, W. Bai, W. Zheng, J. He, G. Sang, Influence of hydrated lime on mechanical and shrinkage properties of alkali-activated slag cement, Constr. Build. Mater. 289 (2021), 123201, https://doi.org/10.1016/j.conbuildmat.2021.123201.

[71] D.P. Bentz, E.J. Garboczi, D.A. Quenard, Modelling drying shrinkage in reconstructed porous materials: application to porous Vycor glass, Model. Simul. Mater. Sci. Eng. 6 (1998) 211.

[72] F. Collins, J. Sanjayan, Effect of pore size distribution on drying shrinking of alkali-activated slag concrete, Cem. Concr. Res. 30 (2000) 1401–1406, https://doi.org/10.1016/S0008-8846(00)00327-6.

[73] T. Lu, Z. Li, H. Huang, Effect of supplementary materials on the autogenous shrinkage of cement paste, Materials 13 (2020) 3367.

[74] C.J. Haecker, E.J. Garboczi, J.W. Bullard, R.B. Bohn, Z. Sun, S.P. Shah, T. Voigt, Modeling the linear elastic properties of Portland cement paste, Cem. Concr. Res. 35 (2005) 1948–1960, https://doi.org/10.1016/j.cemconres.2005.05.001.

[75] Z. Li, B. Delsaute, T. Lu, A. Kostiuchenko, S. Staquet, G. Ye, A comparative study on the mechanical properties and autogenous shrinkage induced stress of alkali-activated concrete and ordinary Portland cement concrete, Constr. Build. Mater. 292 (2021), 123418, https://doi.org/10.1016/j.conbuildmat.2021.123418.

[76] S. Prinsse, Alkali-activated Concrete: Development of Material Properties (Strength And Stiffness) And Flexural Behaviour of Reinforced Beams Over Time, Master Thesis, 2017.

[77] Z. Hu, Early Hydration And Shrinkage of Alkali-activated Slag/Fly Ash Blend Cement, Hunan University, 2013.

[78] T. Lu, Autogenous Shrinkage of Early Age Cement Paste And Mortar, Delft University of Technology, 2019.

[79] A. Kostiuchenko, Z. Li, G. Ye, Experimental study on creep behavior of alkali-activated concrete, in: Int. Conf. Innov. Mater. Sustain. Civ. Eng, 2019, p. 80. Nanjing.

[80] X. Zheng, H. Lu, S. You, K. Cheng, S.M. Easa, Z. Chen, C. Ma, D. Fu, T. Ji, Tensile creep behavior of alkali-activated slag concrete incorporating lightweight aggregate, Constr. Build. Mater. 357 (2022), 129318.

[81] R.J. Myers, E. L'Hôpital, J.L. Provis, B. Lothenbach, Composition-solubility-structure relationships in calcium (alkali) aluminosilicate hydrate (C-(N,K-)A-S-H), Dalton Trans. 44 (2015) 13530–13544, https://doi.org/10.1039/c5dt01124h.

[82] A.E. Naaman, Prestressed Concrete Analysis And Design: Fundamentals, McGraw-Hill New York, 1982.

[83] M.K. Tadros, A. Ghali, W.H. Dilger, Time-dependent prestress loss and deflection in prestressed concrete members, PCI J. 20 (1975) 86–98.
[84] I. Garcia-Lodeiro, A. Palomo, A. Fernández-Jiménez, D.E. MacPhee, Compatibility studies between N-A-S-H and C-A-S-H gels. Study in the ternary diagram Na2O-CaO-Al2O3-SiO2-H2O, Cem. Concr. Res. 41 (2011) 923–931, https://doi.org/10.1016/j.cemconres.2011.05.006.
[85] S. Wilhelm, M. Kind, On the relation between natural and enforced syneresis of acidic precipitated silica, Polymers 6 (2014) 2896–2911.
[86] P. Duxson, J.L. Provis, G.C. Lukey, S.W. Mallicoat, W.M. Kriven, J.S.J. Van Deventer, Understanding the relationship between geopolymer composition, microstructure and mechanical properties, Colloids Surf. A Physicochem. Eng. Asp. 269 (2005) 47–58, https://doi.org/10.1016/j.colsurfa.2005.06.060.
[87] F. Lolli, J.J. Thomas, K.E. Kurtis, Early age volume changes in metakaolin geopolymers: insights from molecular simulations and experiments, Cem. Concr. Res. (2021), 106428, https://doi.org/10.1016/j.cemconres.2021.106428.
[88] Y. Ma, G. Ye, The shrinkage of alkali activated fly ash, Cem. Concr. Res. 68 (2015) 75–82, https://doi.org/10.1016/j.cemconres.2014.10.024.
[89] J. Israelachvili, Chapter 15 - Solvation, Structural, And Hydration Forces, 2011, https://doi.org/10.1016/B978-0-12-375182-9.10015-6.
[90] M. Palacios, S. Gismera, M.M. Alonso, J.B. d'Espinose de Lacaillerie, B. Lothenbach, A. Favier, C. Brumaud, F. Puertas, Early reactivity of sodium silicate-activated slag pastes and its impact on rheological properties, Cem. Concr. Res. 140 (2021), 106302, https://doi.org/10.1016/j.cemconres.2020.106302.
[91] J.N. Israelachvili, H. Wennerström, Entropic forces between amphiphilic surfaces in liquids, J. Phys. Chem. 96 (1992) 520–531, https://doi.org/10.1021/j100181a007.
[92] E.J.W. Verwey, J.T.G. Overbeek, J.T.G. Overbeek, Theory of the Stability of Lyophobic Colloids, Courier Corporation, 1999.
[93] J.N. Israelachvili, Intermolecular And Surface Forces, Academic Press, 2011.
[94] Y. Zuo, M. Nedeljković, G. Ye, Pore solution composition of alkali-activated slag/fly ash pastes, Cem. Concr. Res. 115 (2019) 230–250, https://doi.org/10.1016/j.cemconres.2018.10.010.
[95] Z. Li, Autogenous Shrinkage of Alkali-activated Slag And Fly Ash Materials From Mechanism to Mitigating Strategies, Delft University of Technology, 2021.
[96] X. Zhu, D. Tang, K. Yang, Z. Zhang, Q. Li, Q. Pan, C. Yang, Effect of $Ca(OH)_2$ on shrinkage characteristics and microstructures of alkali-activated slag concrete, Constr. Build. Mater. 175 (2018) 467–482, https://doi.org/10.1016/j.conbuildmat.2018.04.180.
[97] Y. Wang, L. Montanari, W.J. Weiss, P. Suraneni, Internal curing using superabsorbent polymers for alkali activated slag-fly ash mixtures, in: Int. Conf. Appl. Superabsorbent Polym. Other New Admixtures Towar. Smart Concr, 2019, pp. 239–247.
[98] B.S. Gebregziabiher, R.J. Thomas, S. Peethamparan, Temperature and activator effect on early-age reaction kinetics of alkali-activated slag binders, Constr. Build. Mater. 113 (2016) 783–793, https://doi.org/10.1016/j.conbuildmat.2016.03.098.
[99] M. Ben Haha, B. Lothenbach, G. Le Saout, F. Winnefeld, Influence of slag chemistry on the hydration of alkali-activated blast-furnace slag - part I: effect of MgO, Cem. Concr. Res. 42 (2012) 74–83, https://doi.org/10.1016/j.cemconres.2011.08.005.
[100] Y. Zhang, O. Çopuroğlu, Role of the grain size on the hydration characteristics of slag in an aged field concrete, Cem. Concr. Res. 162 (2022), https://doi.org/10.1016/j.cemconres.2022.106985.
[101] H. Ye, A. Radlińska, Shrinkage mitigation strategies in alkali-activated slag, Cem. Concr. Res. 101 (2017) 131–143, https://doi.org/10.1016/j.cemconres.2017.08.025.
[102] B. Chen, J. Wang, J. Zhao, Mitigating the drying shrinkage and autogenous shrinkage of alkali-activated slag by NaAlO2, Materials 13 (2020), https://doi.org/10.3390/MA13163499.
[103] Z. Yang, P. Shi, Y. Zhang, Z. Li, Effect of superabsorbent polymer introduction on properties of alkali-activated slag mortar, Constr. Build. Mater. 340 (2022), 127541, https://doi.org/10.1016/j.conbuildmat.2022.127541.
[104] Japan Society of Civil Engineers (JSCE), Guidelines for Concrete: Standard Specifications for Concrete Structures, 2007.
[105] The International Federation for Structural Concrete (fib), Fib Model Code for Concrete Structures 2010, Ernst & Sohn, Wiley, 2010.
[106] F. Rifai, A. Darquennes, F. Benboudjema, B. Muzeau, L. Stefan, Study of shrinkage restraint effects at early-age in alkali-activated slag mortars, in: 9th Int. Conf. Fract. Mech. Concr. Concr. Struct, 2016, https://doi.org/10.21012/fc9.240. Berkeley, USA.
[107] D. Ravikumar, N. Neithalath, Reaction kinetics in sodium silicate powder and liquid activated slag binders evaluated using isothermal calorimetry, Thermochim. Acta 546 (2012) 32–43, https://doi.org/10.1016/j.tca.2012.07.010.
[108] G. Ye, Experimental Study And Numerical Simulation of the Development of the Microstructure And Permeability of Cementitious Materials, Delft University of Technology, 2003.
[109] F.G. Collins, J.G. Sanjayan, Workability and mechanical properties of alkali activated slag concrete, Cem. Concr. Res. 29 (1999) 455–458.
[110] B. Delsaute, J. Gambacorta, S. Staquet, Influence of the Ms-modulus on the early-age volume change and heat release of slag and fly ash pastes activated by sodium hydroxide and sodium silicate, in: 4th Int. RILEM Conf. Microstruct. Relat. Durab. Cem. Compos, 2020, pp. 781–787.
[111] C. Song, Y.C. Choi, S. Choi, Effect of internal curing by superabsorbent polymers – internal relative humidity and autogenous shrinkage of alkali-activated slag mortars, Constr. Build. Mater. 123 (2016) 198–206, https://doi.org/10.1016/j.conbuildmat.2016.07.007.
[112] G. Pickett, Effect of aggregate on shrinkage of concrete and a hypothesis concerning shrinkage, in: J. Proc, 1956, pp. 581–590.
[113] D.W. Hobbs, Bulk modulus shrinkage and thermal expansion of a two phase material, Nature. 222 (1969) 849–851.
[114] E. Tazawa, R. Sato, E. Sakai, S. Miyazawa, Work of JCI committee on autogenous shrinkage, in: Shrinkage Concr. Shrinkage, 2000, pp. 21–33.
[115] P. Lura, G. Ye, K. van Breugel, Effect of cement type on autogenous deformation of cement-based materials, Spec. Publ. 220 (2004) 57–68.
[116] H. Zhang, B. Šavija, Y. Xu, E. Schlangen, Size effect on splitting strength of hardened cement paste: experimental and numerical study, Cem. Concr. Compos. 94 (2018) 264–276.
[117] W. Lyu, Effect of Micro-cracking And Self-healing on Long-term Creep And Strength Development of Concrete, Delft University of Technology, 2020.
[118] A.M. Neville, Properties of Concrete, Longman, London, 2011.
[119] E. Tazawa, Autogenous Shrinkage of Concrete, CRC Press, 1998.
[120] S.I. Igarashi, A. Bentur, K. Kovler, Autogenous shrinkage and induced restraining stresses in high-strength concretes, Cem. Concr. Res. 30 (2000) 1701–1707, https://doi.org/10.1016/S0008-8846(00)00399-9.
[121] F. Collins, J.G. Sanjayan, Cracking tendency of alkali-activated slag concrete subjected to restrained shrinkage, Cem. Concr. Res. 30 (2000) 791–798, https://doi.org/10.1016/S0008-8846(00)00243-X.
[122] ASTM C 1581, Standard Test Method for Determining Age at Cracking And Induced Tensile Stress Characteristics of Mortar And Concrete Under Restrained Shrinkage, ASTM Int., 2009, pp. 1–7, https://doi.org/10.1520/C1581.
[123] S.J. Lokhorst, Deformational Behaviour of Concrete Influenced by Hydration Related Changes of the Microstructure, Delft University of Technology, 2001.
[124] Z. Li, S. Zhang, X. Liang, G. Ye, Cracking potential of alkali-activated slag and fly ash concrete subjected to restrained autogenous shrinkage, Cem. Concr. Compos. 114 (2020), 103767, https://doi.org/10.1016/j.cemconcomp.2020.103767.
[125] F. Rifai, A. Darquennes, L. Stefan, B. Muzeau, F. Benboudjema, The Analysis of Cracking Risk by Shrinkage Restraint of an Alkali-activated Slag Mortar, MATEC Web Conf, 2020, p. 01038, https://doi.org/10.1051/matecconf/202032201038.
[126] F. Rifai, A. Darquennes, Early-age cracking tendency of alkali-activated slag binders compared to ordinary Portland cement, in: SynerCrete'18 Int. Conf. Interdiscip. Approaches Cem. Mater. Struct. Concr, 2018. Madeira Island.
[127] X. Zhou, Y. Zeng, P. Chen, Z. Jiao, W. Zheng, Mechanical properties of basalt and polypropylene fibre-reinforced alkali-activated slag concrete, Constr. Build. Mater. 269 (2021), 121284.
[128] F. Collins, J.G. Sanjayan, Microcracking and strength development of alkali activated slag concrete, Cem. Concr. Compos. 23 (2001) 345–352, https://doi.org/10.1016/S0958-9465(01)00003-8.
[129] H. Ye, A. Radlińska, Effect of alkalis on cementitious materials: understanding the relationship between composition, structure, and volume change mechanism, J. Adv. Concr. Technol. 15 (2017) 165–177.
[130] J.B.S.A. Bernal, J. Bisschop, J.S.J. van Deventer, J.L. Provis, Drying shrinkage microcracking of alkali-activated slag materials, in: Proc. 34th Annu. Cem. Concr. Sci. Conf. Work. Waste Cem, SA Bernal, JL Provis, 2014, pp. 59–62.
[131] A. Wardhono, C. Gunasekara, D.W. Law, S. Setunge, Comparison of long term performance between alkali activated slag and fly ash geopolymer concretes, Constr. Build. Mater. 143 (2017) 272–279.
[132] S. Prinsse, D.A. Hordijk, G. Ye, P. Lagendijk, M. Luković, Time-dependent material properties and reinforced beams behavior of two alkali-activated types of concrete, Struct. Concr. 21 (2020) 642–658, https://doi.org/10.1002/suco.201900235.
[133] M. Nedeljković, Carbonation Mechanism of Alkali-activated Fly Ash And Slag Materials: In View of Long-term Performance Predictions, Delft University of Technology, 2019.
[134] B. Liu, J. Yang, D. Li, F. Xing, Y. Fang, Effect of a synthetic nano-CaO-Al2O3-SiO2-H2O gel on the early-stage shrinkage performance of alkali-activated slag mortars, Materials 11 (2018), https://doi.org/10.3390/ma11071128.
[135] A.M. Humad, A. Kothari, J.L. Provis, A. Cwirzen, The effect of blast furnace slag/fly ash ratio on setting, strength, and shrinkage of alkali-activated pastes and concretes, Front. Mater. 6 (2019) 1–10, https://doi.org/10.3389/fmats.2019.00009.
[136] W. Sun, K. Hou, Z. Yang, Y. Wen, X-ray CT three-dimensional reconstruction and discrete element analysis of the cement paste backfill pore structure under uniaxial compression, Constr. Build. Mater. 138 (2017) 69–78, https://doi.org/10.1016/j.conbuildmat.2017.01.088.
[137] W. Ren, Z. Yang, R. Sharma, C. Zhang, P.J. Withers, Two-dimensional X-ray CT image based meso-scale fracture modelling of concrete, Eng. Fract. Mech. 133 (2015) 24–39, https://doi.org/10.1016/j.engfracmech.2014.10.016.
[138] D. Marchon, S. Mantellato, A.B. Eberhardt, R.J. Flatt, Adsorption of chemical admixtures, in: Sci. Technol. Concr. Admixtures, Elsevier, 2016, pp. 219–256.
[139] N.P. Mailvaganam, M.R. Rixom, Chemical Admixtures for Concrete, CRC Press, 2002.
[140] N.S. Berke, L. Li, M.C. Hicks, J. Bae, Improving concrete performance with shrinkage-reducing admixtures, Spec. Publ. 217 (2003) 37–50.
[141] X. Hu, C. Shi, Z. Zhang, Z. Hu, Autogenous and drying shrinkage of alkali-activated slag mortars, J. Am. Ceram. Soc. (2019) 1–13, https://doi.org/10.1111/jace.16349.
[142] M. Palacios, F. Puertas, Effect of shrinkage-reducing admixtures on the properties of alkali-activated slag mortars and pastes, Cem. Concr. Res. 37 (2007) 691–702.

[143] L. Kalina, E.B. Ková, J. Krouská, V.B. Jr., Polypropylene Glycols as Effective Shrinkage-Reducing Admixtures in Alkali-Activated Materials, Mater. J. 115 (n. d.). doi:10.14359/51701099.
[144] V. Bilek Jr., L. Kalina, O. Fojtík, Shrinkage-reducing admixture efficiency in alkali-activated slag across the different doses of activator, in: Key Eng. Mater, Trans Tech Publ, 2018, pp. 19–22.
[145] T. Bakharev, J.G. Sanjayan, Y.B. Cheng, Effect of admixtures on properties of alkali-activated slag concrete, Cem. Concr. Res. 30 (2000) 1367–1374, https://doi.org/10.1016/S0008-8846(00)00349-5.
[146] M. Palacios, F. Puertas, Effect of superplastisizer and shrinkage reducing admixtures on alkali-activated slag pastes and mortars, Cem. Concr. Res. 35 (2005) 1358–1367, https://doi.org/10.1016/j.cemconres.2004.10.014.
[147] P. Lura, O.M. Jensen, K. Van Breugel, Autogenous shrinkage in high-performance cement paste: an evaluation of basic mechanisms, Cem. Concr. Res. 33 (2003) 223–232, https://doi.org/10.1016/S0008-8846(02)00890-6.
[148] J. Yang, D. Snoeck, N. De Belie, Z. Sun, Effect of superabsorbent polymers and expansive additives on the shrinkage of alkali-activated slag, Cem. Concr. Compos. 123 (2021), 104218, https://doi.org/10.1016/j.cemconcomp.2021.104218.
[149] C. Li, H. Shi, W. Zhou, J. Cha, J. Huang, W. Shen, Influence of the thermal treatment process of MgO on alkali-activated cement, Bull. Chin. Ceram. Soc. 35 (2016) 632–637 (In Chinese).
[150] Y. Yang, Z. Li, X. Zhang, J. Wei, Q. Yu, Reaction mechanism of compensating shrinkage of inorganic polymer pastes by using reactive MgO, J. South China Univ. Technol. (Nat. Sci. Ed.) 45 (2017) 102–109 (In Chinese).
[151] L.Y. Yang, Z.J. Jia, Y.M. Zhang, J.G. Dai, Effects of nano-TiO2on strength, shrinkage and microstructure of alkali activated slag pastes, Cem. Concr. Compos. 57 (2015) 1–7, https://doi.org/10.1016/j.cemconcomp.2014.11.009.
[152] H. Chen, M. Wyrzykowski, K. Scrivener, P. Lura, Prediction of self-desiccation in low water-to-cement ratio pastes based on pore structure evolution, Cem. Concr. Res. 49 (2013) 38–47, https://doi.org/10.1016/j.cemconres.2013.03.013.
[153] V. Mechtcherine, M. Gorges, C. Schroefl, A. Assmann, W. Brameshuber, A. B. Ribeiro, D. Cusson, J. Custódio, E.F. Da Silva, K. Ichimiya, S.I. Igarashi, A. Klemm, K. Kovler, A.N. De Mendonça Lopes, P. Lura, V.T. Nguyen, H. W. Reinhardt, R.D.T. Filho, J. Weiss, M. Wyrzykowski, G. Ye, S. Zhutovsky, Effect of internal curing by using superabsorbent polymers (SAP) on autogenous shrinkage and other properties of a high-performance fine-grained concrete: results of a RILEM round-robin test, Mater. Struct. 47 (2014) 541–562, https://doi.org/10.1617/s11527-013-0078-5.
[154] O.M. Jensen, P.F. Hansen, Water-entrained cement-based materials - I. Principles and theoretical background, Cem. Concr. Res. 31 (2001) 647–654, https://doi.org/10.1016/S0008-8846(01)00463-X.
[155] P. Lura, F. Durand, O.M. Jensen, Autogenous strain of cement pastes with superabsorbent polymers, in: Proc. Internaltional RILEM Conf. Vol. Chang. Hardening Concr. Test. Mitig. C, 2006, pp. 57–66, https://doi.org/10.1617/2351580052.007.
[156] J. Justs, M. Wyrzykowski, D. Bajare, P. Lura, Internal curing by superabsorbent polymers in ultra-high performance concrete, Cem. Concr. Res. 76 (2015) 82–90, https://doi.org/10.1016/j.cemconres.2015.05.005.
[157] D. Snoeck, O.M. Jensen, N. De Belie, The influence of superabsorbent polymers on the autogenous shrinkage properties of cement pastes with supplementary cementitious materials, Cem. Concr. Res. 74 (2015) 59–67, https://doi.org/10.1016/j.cemconres.2015.03.020.
[158] Z. Li, X. Yao, Y. Chen, T. Lu, G. Ye, A low-autogenous-shrinkage alkali-activated slag and fly ash concrete, Appl. Sci. 10 (2020) 6092, https://doi.org/10.3390/app10176092.
[159] A.R. Sakulich, D.P. Bentz, Mitigation of autogenous shrinkage in alkali activated slag mortars by internal curing, Mater. Struct. 46 (2013) 1355–1367, https://doi.org/10.1617/s11527-012-9978-z.
[160] M. Ben Haha, G. Le Saout, F. Winnefeld, B. Lothenbach, Influence of activator type on hydration kinetics, hydrate assemblage and microstructural development of alkali activated blast-furnace slags, Cem. Concr. Res. 41 (2011) 301–310, https://doi.org/10.1016/j.cemconres.2010.11.016.
[161] G.Z. Zhang, X.Y. Wang, T.W. Kim, J.Y. Lim, Y. Han, The effect of different types of internal curing liquid on the properties of alkali-activated slag (Aas) mortar, Sustainability 13 (2021) 1–16, https://doi.org/10.3390/su13042407.
[162] Z. Yang, P. Shi, Y. Zhang, Z. Li, Influence of liquid-binder ratio on the performance of alkali-activated slag mortar with superabsorbent polymer, J. Build. Eng. 48 (2022), 103934, https://doi.org/10.1016/j.jobe.2021.103934.
[163] D. Snoeck, C. Schröfl, V. Mechtcherine, Recommendation of RILEM TC 260-RSC: testing sorption by superabsorbent polymers (SAP) prior to implementation in cement-based materials, Mater. Struct. 51 (2018) 116, https://doi.org/10.1617/s11527-018-1242-8.
[164] C. Fu, H. Ye, A. Lei, G. Yang, P. Wan, Effect of novel superabsorbent polymer composites on the fresh and hardened properties of alkali-activated slag, Constr. Build. Mater. 232 (2020), 117225, https://doi.org/10.1016/j.conbuildmat.2019.117225.
[165] V. Mechtcherine, D. Snoeck, C. Schröfl, N. De Belie, A.J. Klemm, K. Ichimiya, J. Moon, M. Wyrzykowski, P. Lura, N. Toropovs, A. Assmann, S. ichi Igarashi, I. De La Varga, F.C.R. Almeida, K. Erk, A.B. Ribeiro, J. Custódio, H.W. Reinhardt, V. Falikman, Testing superabsorbent polymer (SAP) sorption properties prior to implementation in concrete: results of a RILEM Round-Robin Test, Mater. Struct. 51 (2018), https://doi.org/10.1617/s11527-018-1149-4.
[166] N.K. Lee, S.Y. Abate, H.K. Kim, Use of recycled aggregates as internal curing agent for alkali-activated slag system, Constr. Build. Mater. 159 (2018) 286–296, https://doi.org/10.1016/j.conbuildmat.2017.10.110.
[167] G.Z. Zhang, H.S. Lee, X.Y. Wang, Y. Han, Internal curing effect of pre-soaked zeolite sand on the performance of alkali-activated slag, Materials 14 (2021) 1–14, https://doi.org/10.3390/ma14040718.
[168] P. Chen, J. Wang, L. Wang, Y. Xu, Perforated cenospheres: a reactive internal curing agent for alkali activated slag mortars, Cem. Concr. Compos. 104 (2019), 103351, https://doi.org/10.1016/j.cemconcomp.2019.103351.
[169] B. Fu, Z. Cheng, J. Han, N. Li, Understanding the role of metakaolin towards mitigating the shrinkage behavior of alkali-activated slag, Materials 14 (2021) 1–19, https://doi.org/10.3390/ma14226962.
[170] C. Zhu, Y. Zhou, Y. Guo, Z. Wen, L. Zhang, Z. Wang, Y. Fang, W. Long, Resistivity measurements to study the early chemical and autogenous shrinkage of a binary alkali-activated slag-metakaolin system, IOP Conf. Ser. Earth Environ. Sci. 791 (2021), https://doi.org/10.1088/1755-1315/791/1/012146.
[171] J. Davidovits, Geopolymer Chemistry & Applications, 4th ed., Institut Géopolymère, Saint-Quentin, France, 2015.
[172] S.A. Bernal, J.L. Provis, V. Rose, R. Mejía De Gutierrez, Evolution of binder structure in sodium silicate-activated slag-metakaolin blends, Cem. Concr. Compos. 33 (2011) 46–54, https://doi.org/10.1016/j.cemconcomp.2010.09.004.
[173] S.A. Bernal, R. Mejía De Gutiérrez, J.L. Provis, Engineering and durability properties of concretes based on alkali-activated granulated blast furnace slag/metakaolin blends, Constr. Build. Mater. 33 (2012) 99–108, https://doi.org/10.1016/j.conbuildmat.2012.01.017.
[174] T. Bakharev, J.G. Sanjayan, Y. Cheng, Effect of elevated temperature curing on properties of alkali-activated slag concrete, Cem. Concr. Res. 29 (1999) 1619–1625.
[175] ASTM C1698, Standard Test Method for Autogenous Strain of Cement Paste And Mortar, 2013, pp. 1–8, https://doi.org/10.1520/C1698-09.2.
[176] K. Orosz, A. Humad, H. Hedlund, A. Cwirzen, Autogenous deformation of alkali-activated blast furnace slag concrete subjected to variable curing temperatures, Adv. Civ. Eng. 2019 (2019) 1–8, https://doi.org/10.1155/2019/6903725.
[177] M. Alexa, D. Kocáb, B. Kucharczyková, J. Kotrla, Experimental determination of early shrinkage of alkali-activated slag, Solid State Phenom. 292 SSP (2019) 114–119, https://doi.org/10.4028/www.scientific.net/SSP.292.114.
[178] M. Chang-wen, T. Qian, S. Wei, L. Jia-ping, Water consumption of the early-age paste and the determination of “time-zero” of self-desiccation shrinkage, Cem. Concr. Res. 37 (2007) 1496–1501, https://doi.org/10.1016/j.cemconres.2007.08.005.
[179] M. Wyrzykowski, Z. Hu, S. Ghourchian, K. Scrivener, P. Lura, Corrugated tube protocol for autogenous shrinkage measurements: review and statistical assessment, Mater. Struct. 50 (2017) 57, https://doi.org/10.1617/s11527-016-0933-2.
[180] NEN-EN 196-3 + A1, Methods of Testing Cement - Part 3: Determination of Setting Times And Soundness, 2016.
[181] C. Liu, X. Liang, Y. Chen, Z. Li, G. Ye, Degradation of alkali-activated slag subject to water immersion, Cem. Concr. Compos. (2023), 105157.
[182] ASTM C191-18a, Standard Test Methods for Time of Setting of Hydraulic Cement by Vicat Needle, 2019, pp. 1–8, https://doi.org/10.1520/C0191-18A.2.
[183] E. Beerda, In Friesland durven ze het aan: een autobrug van beton zonder een gram cement, Cobouw, Oct 26, https://www.cobouw.nl/duurzaamheid/nieuws/2021/10/in-friesland-durven-ze-het-aan-een-autobrugdek-van-beton-zonder-cement-101299832#.YXkNZH91I1M.linkedin, 2021.
[184] K. Yang, C. Yang, J. Zhang, Q. Pan, L. Yu, Y. Bai, First structural use of site-cast, alkali-activated slag concrete in China, Proc. Inst. Civ. Eng. Build. 171 (2018) 800–809.
[185] B.S. Gebregziabiher, R. Thomas, S. Peethamparan, Very early-age reaction kinetics and microstructural development in alkali-activated slag, Cem. Concr. Compos. 55 (2015) 91–102, https://doi.org/10.1016/j.cemconcomp.2014.09.001.
[186] H. Huang, G. Ye, Examining the “time-zero” of autogenous shrinkage in high/ultra-high performance cement pastes, Cem. Concr. Res. 97 (2015) 107–114, https://doi.org/10.1016/j.cemconres.2017.03.010.
[187] O.M. Jensen, Autogenous Deformation And RH-change—Self-desiccation And Self-desiccation Shrinkage (in Danish, Phd Thesis) Vol. 285, Build. Mater. Lab. Tech. Univ. Denmark, Lyngby, Denmark, 1993.
[188] Z. Hu, M. Wyrzykowski, P. Lura, Estimation of reaction kinetics of geopolymers at early ages, Cem. Concr. Res. 129 (2020), 105971, https://doi.org/10.1016/j.cemconres.2020.105971.
[189] S. Uppalapati, L. Vandewalle, Ö. Cizer, Monitoring the setting process of alkali-activated slag-fly ash cements with ultrasonic P-wave velocity, Constr. Build. Mater. 271 (2021), 121592.
[190] B. Delsaute, C. Boulay, J. Granja, J. Carette, M. Azenha, C. Dumoulin, G. Karaiskos, A. Deraemaeker, S. Staquet, Testing concrete E-modulus at very early ages through several techniques: an inter-laboratory comparison, Strain. (2016) 91–109, https://doi.org/10.1111/str.12172.
[191] P. Lura, K. Van Breugel, I. Maruyama, Effect of curing temperature and type of cement on early-age shrinkage of high-performance concrete, Cem. Concr. Res. 31 (2001) 1867–1872, https://doi.org/10.1016/S0008-8846(01)00601-9.
[192] T. Lu, Z. Li, K. Van Breugel, Numerical modelling of autogenous shrinkage of hardening cement paste, Constr. Build. Mater. 264 (2020), 120708, https://doi.org/10.1016/S0008-8846(97)00170-1.
[193] S. Zhutovsky, K. Kovler, A. Bentur, Efficiency of lightweight aggregates for internal curing of high strength concrete to eliminate autogenous shrinkage, Mater. Struct. 35 (2002) 97–101.
[194] O. Nanayakkara, C. Gunasekara, M. Sandanayake, D.W. Law, K. Nguyen, J. Xia, S. Setunge, Alkali activated slag concrete incorporating recycled aggregate

concrete: long term performance and sustainability aspect, Constr. Build. Mater. 271 (2021), 121512.
[195] A. Allahverdi, B. Shaverdi, E.N. Kani, Influence of sodium oxide on properties of fresh and hardened paste of alkali-activated blast-furnace slag, Int. J. Civ. Eng. 8 (2010) 304–314.
[196] R. Cao, B. Li, N. You, Y. Zhang, Z. Zhang, Properties of alkali-activated ground granulated blast furnace slag blended with ferronickel slag, Constr. Build. Mater. 192 (2018) 123–132, https://doi.org/10.1016/j.conbuildmat.2018.10.112.
[197] K. Yin, Y. Jiang, H. He, J. Ren, Z. Li, Characterization of one-part alkali-activated slag with rice straw ash, Constr. Build. Mater. 345 (2022), 128403, https://doi.org/10.1016/j.conbuildmat.2022.128403.
[198] N. You, B. Li, R. Cao, J. Shi, C. Chen, Y. Zhang, The influence of steel slag and ferronickel slag on the properties of alkali-activated slag mortar, Constr. Build. Mater. 227 (2019), 116614, https://doi.org/10.1016/j.conbuildmat.2019.07.340.
[199] S. Oh, Y.C. Choi, Superabsorbent polymers as internal curing agents in alkali activated slag mortars, Constr. Build. Mater. 159 (2018) 1–8, https://doi.org/10.1016/j.conbuildmat.2017.10.121.
[200] S. Uppalapati, Ö. Cizer, Assessing the autogenous shrinkage of alkali- activated slag/fly ash mortar blends, in: ACI Spec. Publ. 2017-Janua, Am. Concr. Institute, 2017.
[201] F. Rifai, A. Darquennes, F. Benboudjema, B. Muzeau, L. Stefan, Thermo-chemo-mechanical behavior of alkali-activated slag materials - focus on early-age, in: 2nd Int. RILEM/COST Conf. Early Age Crack. Serv. Cem. Mater. Struct. - EAC2, 2017. Brussels.
[202] Z. Li, S. Zhang, Y. Zuo, W. Chen, G. Ye, Chemical deformation of metakaolin based geopolymer, Cem. Concr. Res. 120 (2019) 108–118, https://doi.org/10.1016/j.cemconres.2019.03.017.
[203] Z. Li, P. Gao, G. Ye, Experimental study on autogenous deformation of metakaolin based geopolymer, in: 2nd Int. RILEM/COST Conf. Early Age Crack. Serv. Cem. Mater. Struct, 2017, pp. 209–214. Brussels.